INTERACTION BETWEEN CRACKS, DISLOCATIONS AND INCLUSIONS - APPLICATION TO HIGH-STRAIN-RATE DEFORMATION PHENOMENA

A Thesis Submitted
In Partial Fulfilment of the Requirements
for the Degree of

M. Tech

By

Pradeep Kumar Varma

to the

DEPARTMENT OF MATERIALS & METALLURGICAL ENGINEERING

INDIAN INSTITUTE OF TECHNOLOGY KANPUR

April, 1994

To my parents

CERTIFICATE

This is to certify that the thesis work entitled "**INTERACTION BETWEEN MOVING CRACKS, DISLOCATIONS AND INCLUSIONS - APPLICATIONS TO HIGH-STRAIN-RATE DEFORMATION PHENOMENA**", being submitted by **Mr. PRADEEP KUMAR VARMA** in partial fulfillments of the requirement for the award of the degree of **MASTER OF TECHNOLOGY** in Metallurgical and Materials Engineering at **I.I.T. KANPUR** is a record of candidates own work carried out by him under my supervision and guidance during period 1992-94.

This thesis work had not been submitted else where for a degree.

(M.N.SHETTY)

PROFESSOR

Deptt. of Materials and Metallurgical Engineering

I.I.T. KANPUR

KANPUR - 208016(U.P.)

INDIA

ACKNOWLEDGEMENT

I owe my profound gratitude to **Dr. M. N. SHETTY** for his valuable guidance, supervision, persistent encouragement and informative discussions at every stage in preparation of this reports.

Thanks are due to other who have helped in improving the overall getup of the thesis work.

(PRADEEP KUMAR VARMA)

CONTENTS

LIST OF FIGURES

LIST OF TABLES

LIST OF SYMBOLS

$\dot{a}$	Speeds of crack tip
$a(t)$	Displacement function; continuous function of time
b	Burger vector of dislocation
c_1	Elastic dilatational wave speed
c_2	Elastic shear wave speed
c_R	Elastic Rayleigh surface wave speed
d	polar coordinate of dislocation
D	The quantity $4\,\delta_1\,\delta_2 - (1+\delta_2^2)^2$; a function of crack tip speeds
E	Young's elastic modulus
E_c	Total strain energy per unit length of crack front
E_c^m	Total strain energy per unit length of moving crack front
E_c^s	Total strain energy per unit length of static crack front
$E_{c\to d}$	Crack to dislocation interaction energy
$E_{d\to c}$	Dislocation to crack interaction energy
E_{c-d}	Interaction energy between crack and dislocation
F	Force on a dislocation
$f(\theta)$	The quantity a function of angle θ
$f_{ij}(\theta,\dot{a})$	The quantity a function of angle θ and crack speeds $\dot{a}$.
G	Elastic shear modulus for α-Fe
K_I	Stress intensity factor
n	Number of dislocation
P_{ij}	Components of stress tensor for moving dislocation
r	polar coordinate for crack
r,ψ,ϕ	Spherical coordinate

r_i	The quantities $r\left[1 - \left(1 - \delta_i^2 \right)\sin^2\theta \right]^{1/2}$; $i = 1,2$
r°	Radius of inclusion
r'	Radius of interstitial site
R^*	Core radius for crack tip region
$r_\circ$	Core radius of dislocation
R	Distance from crack tip to the boundary of medium
to	The quantity $\frac{G}{2\pi(1-\nu)}$
Um	Elastic interaction energy for moving crack-inclusion interaction
Us	Elastic interaction energy for static crack-inclusion interaction
Ui	Elastic interaction energy for dislocation-inclusion interaction
U_c	Strain energy density
U_c^m	Strain energy density for moving crack
U_c^s	Strain energy density for static crack
U	Total strain energy per unit length of edge dislocation
U_d^m	Strain energy density of moving dislocation
U_I	Total strain energy of an inclusion
x,y,z	Rectangular coordinate
x',y',z'	Rectangular coordinate
ν	poisson's ratio
μ	Elastic shear modulus for inclusion
ρ	Mass density of matrix α-Fe
v	Dislocation velocity
γ_i	The quantities $\left[1 - \left(1 - \delta_i^2 \right)\sin^2\theta \right]^{1/2}$; $i = 1,2$
ε	Misfit strain
ξ,ζ_i	Rectangular coordinate

θ Polar coordinate

β Polar coordinate

θ_i The quantities $\tan^{-1}\left(\delta_i \tan\theta\right)$; $i = 1,2$

σ_{ij} Components of stress tensor

σ'_{ij} Components of transform crack tip stress tensor

$\sigma^{d'}_{ij}$ Components of stress tensor for dislocation

σ^{d}_{ij} Transform cgmponents of stress tensor for dislocation

ε_{ij} Components of strain tensor

ε^{c}_{ij} Elastic strain tensor for crack

α_{ij} Components of direction cosines

ω The quantity $\left[1 - \frac{v^2}{2\ c_2^2}\right]$

δ_1 The quantity $\left[1 - \left(\frac{\delta}{c_1}\right)^2\right]^{1/2}$

δ_2 The quantity $\left[1 - \left(\frac{\delta}{c_2}\right)^2\right]^{1/2}$

δ_3 The quantity $\left[1 - \left(\frac{v}{c_1}\right)^2\right]^{1/2}$

δ_4 The quantity $\left[1 - \left(\frac{v}{c_2}\right)^2\right]^{1/2}$

α Correction factor

LIST OF ABBREVIATIONS

DFZ	Dislocation-Free Zone
BCS	Bilby, Cottrell and Swinden
TEM	Transmission Electron Microscopy
MSED	Minimum Strain Energy density
LiF	Lithium Floride
Al_2O_3	Alumina
SiO_2	Silicon Oxide
MnO	Maganege Oxide

ABSTRACT

The evolution of dislocation sub-structure ahead of a moving crack tip with or without the presence of a spherical inclusion is examined in mode I cracking using isotropic elasticity. This is done by considering the glide force on an edge dislocation located at the crack tip moving at speeds in the range $0 < \dot{a} < c_R$ and $c_R < \dot{a} < c_2$, where c_R and c_2 are the Rayleigh wave speed and shear wave speed, respectively. Since the glide force on the edge dislocation is determined by the σ_{12} component of the crack stress field, the angular dependence of σ_{12} is examined at fixed radial vector from the moving crack tip. The transformed σ_{12} component of crack stress has maximum value in the direction $\theta \cong 70^{\circ}$ for the crack tip velocity less than or equal to $0.2c_2$. For crack tip velocities in the range $0.2c_2 < \dot{a} < 0.8c_2$, maximum is located in a direction perpendicular to the motion of crack tip($\theta \cong 90^{\circ}$). For velocities greater than or equal to $0.8c_2$, there are two maxima. The first maximum of greater magnitude is located along $\theta \cong 90^{\circ}$ for all speeds greater than or equal to $0.8c_2$. The second maximum of smaller magnitude is located along $\theta \cong 30^{\circ}$ at $0.8c_2$ and along $\theta \cong 40^{\circ}$ in velocities range $0.9c_2 \leq \dot{a} < c_R$. For velocities range $c_R < \dot{a} < c_2$ the second maximum is located along $\theta \cong 50^{\circ}$.

The effect of inclusion on crack-dislocation interaction is separately examined. The strain energy density for crack and dislocation, and the interaction energy for crack-dislocation, crack-inclusion and dislocation-inclusion combinations have been calculated. The crack propagation characteristics are analyzed by considering the strain energy density of the crack and the

generation on active slip systems located on the maximum of the shear stress lobes is obtained by matching the strain energy density of an equivalent bundle of dislocations produced from a source to that of the moving crack. This is then incorporated into a sub-structure evolution model around a moving crack.

CHAPTER 1

1. INTRODUCTION

The field of fracture mechanics deals with the description of a deformable body containing a crack or cracks and also characterizing and measuring the resistance of materials to crack growth. Excellent review of the subject had appeared in standard text by Knott[13], Broek[48], Hellen[39] and Parton and Morozor[49] and in a number of ASTM STP Proceedings. The dynamic fracture mechanics which is a sub-branch of fracture mechanics examines the behavior of moving crack and is applicable to failure in high strain rate deformation phenomena like impact loading and explosive forming.In these processes crack move at a range of subsonic velocities and hence their propagation characteristics are different than at normal velocities. The static equilibrium conditions of Griffith[40] and Irwin-Orowan[41] may no longer be valid for dynamic processes.

There are two ways in which a crack system may become dynamic. The first type arises when a crack reaches a point of instability in its length where the system acquires kinetic energy by virtue of the inertia of the material surrounding the rapidly separating crack walls. Such a dynamic state may be realized even under fixed loading conditions. The second type of dynamic state arises when the applied loading is subjected to a rapid time variation , as in impact loading. In both cases, the deposition and or transmission of the energy to the crack tip takes place through shock or other mode of wave motion. The stress fields in the material is highly concentrated at the crack tip such that the externally applied stress is many orders of magnitude lower than

that necessary to break the bonds. As the crack propagates in a medium which inherently contains a number of microstructural inhomogeneities such as inclusions and dislocations, the following interaction arises: (i) crack-dislocation, (ii) crack-inclusion and (iii) a combination of (i) and (ii), all of which can alter the propagation characteristics of the crack by directly affecting the crack driving force. Cracks also act as a important source of dislocation generation because of the crack tip plasticity associated with a crack. In this work a numerical calculation of these interactions between moving cracks, dislocations and inclusions is undertaken with possible applications to sub-structure evolution and failure in high strain rate deformation phenomena. A related dislocation problem and the resultant sub-structure evolution under dynamic conditions has been examined by Shetty[55].

1.1 MODES OF CRACK PROPAGATION:

In continuum stress analysis for plane cracks three basic 'modes' of cracks have been identified. Mode I (*opening mode*) corresponds to normal separation of the crack faces under the action of the tensile stresses; mode II (*sliding mode*) corresponds to longitudinal shearing of the crack faces in a direction normal to the crack front; mode III (*tearing mode*) corresponds to lateral shearing parallel to the crack front.Extensions in the shear modes II and III bear a certain analogy to the glide motions of the edge and the screw dislocations. Of the three modes, the mode I is the most predominant to crack propagation in highly brittle solids. There is always a tendency for a brittle crack to have an orientation

that minimizes the the shear loading. Mode I is the most important for practical applications, although the other modes and combinations of modes I and II do occur. In our discussion, we only consider the mode I type crack propagation.

1.2 DUCTILE-BRITTLE FRACTURE:

The most simple definitions for ductile and brittle fracture available in literature are: Fracture accompanied by substantial plastic deformation, called ductile fracture and fracture without any observable plastic deformation by naked eye,called brittle fracture. But at atomistic level plastic deformation is also observed in case of brittle fracture. The extent of plastic deformation in brittle fracture is smaller as compared to ductile fracture. Hence two types of fracture can be distinguished on the basis of the extent of plastic deformation associated with crack propagation. The more scientific definition given by Rice and Thomson [2] is that a material is intrinsically brittle if it can sustain an atomically sharp crack without shear breakdown and dislocation emission. A material is intrinsically ductile if it is vice versa. A sharp crack is stable in metals and other materials that possess dislocation sources close enough to create a dislocation screen which shields the crack fronts from the external stress fields. If the crack is completely unstable,then a sharp crack will breakdown under stress by continuous dislocation emission and the crack will open with a notch of finite angle equal to the angle between a active slip plane.[1]

Under dynamic loading conditions the balance between ductile-brittle or the cleavage-emission balance may alter. For

example, the ductile-brittle transition in steel depends on the strain rate[13]. The recent experiments on ductile copper alloys which suggest that cleavage can be generated by stress corrosion at the crack tip [12]. This is in contrast to the fundamental understanding regarding fracture, because copper is completely ductile under normal conditions. Sieradzki *et al.*[11] have proposed that the cracks are generated by the formation of a brittle sponge at the crack tip during the corrosion reaction at the tip. Lin and Thomson [10] have proposed that there exists a critical velocity above which the driving crack tip stress field is sufficient to overwhelm the maximum induced shielding provided by any emitted dislocation. Ashby and Embury [9] have suggested that in the bcc metals, the response is determined by the nature of the force laws at the crack tip. In their view the sufficient number of dislocations near the crack tip can be activated to move fast enough to intersect and blunt the crack before the crack moves on and this leads to an overall ductility. Hart [8] has shown that a crack shows a brittle transition at a critical velocity, when that crack generates dislocation shielding and the inability of the dislocation generation to keep up with the crack as the crack speeds up.

1.3 CRACK-DISLOCATION INTERACTION:

The brittle fracture in some structural materials is followed by plastic deformation and that some crack tip deformation occurs during the rapid crack propagation. Question arises how the mode of crack tip deformation is controlled and how it is related to the onset of brittle fracture. To understand these questions, it is necessary to understand the manner in which

they interact with cracks during crack propagation. This interaction is also expected to determine whether a crack tip is to serve as the main source of dislocation. This is important because the dislocation emitted from the crack tip shields the crack from the applied stress, thereby reducing the local stress intensity factor. Dislocations generated from other sources do not necessarily shield the crack tip.

Theoretical analysis of crack-dislocation interaction was reported by Louat[7] who used a dislocation model for a finite, double-ended, two-dimensional crack interacting with a parallel screw dislocation outside the crack in an isotropic medium. The same problem for the semi-infinite crack was solved by Asaro[35] and Majumdar and Burns[20] by conformal mapping. Also in isotropic medium, Rice and Thomson[2] formulated the interaction between a dislocation of general Burger vector and a crack by a thermodynamic technique. In anisotropic media, Atkinson [3] and latter Bernett and Asaro[6] presented procedures for solving the elastic problem involving a crack and a dislocation.

The recent renewed interest of dislocation-crack interaction arises from the realization that a critical stress intensity factor may by needed for dislocation emission from the crack [2], because of such a critical stress intensity factor, the dislocation distribution emitted from the crack in either the mode I or the mode II or III situation would be different from those obtained previously without such a factor[4-5]. The most important difference is the existence of a dislocation free zone(DFZ) [1,14] near the tip of crack. In fact it was the observation of the DFZ stimulated the interests in the

dislocation-crack interaction because of the fact that a dislocation emitted from a crack shields the crack tip from the applied stress, emission process must be intermittent and the time and size of the plastic zone depends on the mobility of dislocation.

Louat[7] had made a quantitative examination of the elastic interaction of cracks and screw dislocation and found out that the number of dislocations which can be caused to enter the crack and the energy of the crack-dislocation pair. The tendency for the crack propagation increases as the number of dislocation within it increases. Warren[36] use plane strain linear elasticity theory to develop full field expressions for forces on edge and screw dislocations in an infinite elastic plane containing an elliptical shaped stress free hole and under limiting geometric conditions had shown that an edge dislocation with Burger vector normal to the crack front, moved away from the crack tip and those with Burger vector parallel to the crack front, accumulated at the crack tip.

1.3.1 DISLOCATION-FREE ZONE (DFZ):

Bilby et al.[4] found out dislocation distribution emitted from the two ends of a double-ended crack in the mode II or III situations and shown that there was no barrier for dislocation emission. As a result, when the crack had emitted all the possible dislocations, the stress intensity factor at the tip of the crack becomes zero. Using similar criterion, the emission of four arrays of edge dislocation in the mode I was studied by Vitek[15] using the interaction of an edge dislocation with a crack and by Riedel[5] using the dislocation model for a crack. In

all these cases the dislocation density approached infinity at the crack tip.

The Bilby, Cottrell and Swinden model(BCS)[4] dose not allow crack growth caused by shielding of dislocation pile-ups at crack tip. The problems associated with the BCS model are due to the absence of an energy barrier for dislocation emission from crack tip. The Ohr and Chang[16,17] assume a DFZ near crack tip and found out a new distribution different from the BCS[[4]. Between the crack tip and plastic zone, there is a region free from dislocation, which is referred to as the dislocation free zone. In this new distribution, the distribution function started from zero at one end of the DFZ increases to a maximum and decreases to zero again at the end of the plastic zone. The stress intensity factor at the crack tip was no longer zero and depends on the length of the DFZ The K_I at the crack tip would be zero only if the DFZ was absent. The same type of solution was found by Majumdar and Burns [18] for a semi-infinite crack. Rice and Thomson[2] in analyzing the dislocation-crack interaction suggested that there should be a barrier to dislocation emission. With a barrier the equilibrium distribution is such that there is a DFZ at the crack tip. One such barrier is the image stress on a dislocation.

The DFZ near crack tip was observed by[1,14] in transmission electron microscopy(TEM). Chia and Burns[34] have observed distribution of dislocations ahead of a crack tip in bulk single crystal of LiF using the etch pits technique under mode I loading condition and found that the maximum density of dislocations was located approximately 6-10 μm in front of the

crack tip. This implies that there is a DFZ in the immediate vicinity of the crack tip. This observation is in agreement with the results of in *situ* TEM studies[1].

1.3.2 DISLOCATION EMISSION:

The direct observation of dislocation emissions from crack tip are confirmed by Kobayshi and Ohr[1], who did in *situ* shear cracking (mode III) experiments on their foil of Mo and W, Ohr and Narayan[19] on similar experiments in stainless steel and Majumdar and Burns [20] who showed dislocations at crack tip in bulk MgO revealed by TEM after thinning. The dislocation distribution near the crack tip revealed a region free of dislocation next to the crack and this was attributed to The attraction between the crack and its emitted dislocations[20].

Chia and Burns[34] in their experimental etch pit studies, under mode I loading conditions, choose the crystal orientation such that the cracks were made to propagate along the {100} as well as the {110} planes. Experiments reveal that the edge dislocations were emitted on two symmetrically inclined slip planes. The slip planes intersect the crack plane along the crack front. The Burger vectors of these dislocations had a component normal to the crack plane and hence these dislocation blunted the crack tip during emission. The second type of crack tip geometry observed consists of arrays of screw dislocations on two mutually perpendicular slip planes that intersected the crack plane at 45^{o}. They concluded that crack tip was again the source of the dislocations. These dislocations intersected ahead of the crack tip and formed sessile dislocations of a <100> type, which could impede crack propagation. These dislocations do not blunt the

crack tip but rather cause the crack front to jog.

Rice and Thomson[2] proposed that if the applied stress is sufficiently high so that the attractive interaction is less than or equal to the core radius(r_o) of a dislocation then the emerging dislocation will always be on the repulsive side of the force distance curve. The dislocation is emitted spontaneously in this situation. In addition, as suggested by Bilby et at.[4], the force on the dislocation must be greater than the lattice friction force, $b\sigma_f$, in order for the dislocation to glide away from the crack. The dislocation emission condition proposed by Thomson[21] and Lin and Thomson[22] is that the combined stress intensity factor (included all the three modes), should be greater than or equal to some critical stress intensity factor for dislocation emission. For a moving crack number of dislocations emitted at the steady state is smaller than the equilibrium number emitted from a stationary crack. The faster the crack moves, the smaller is the steady state number. Also for a moving crack there are saturation numbers even at zero lattice friction (no saturation for stationary crack) and with increasing lattice friction, the effect of crack motion diminishes. The moving crack also has a smaller plastic zone size (the distance between the farthest dislocation and the crack tip). After each emission, the crack stops momentarily because of a sudden reduction of K_I. After the emitted dislocation moves away, the crack speeds up again until K_I increases to some critical value [57].

In mode II and III, edge and screw dislocations respectively, are emitted on slip planes that are nearly coplanar to the crack plane. In these instances, the crack tip remained

sharp, since Burger vector is parallel to the crack plane.Cracks often propagation in a zig-zag manner[19]. In this process a crack propagating along a path suddenly stopped. It could be seen that many of the dislocations emitted from the crack tip are piled up ahead of the crack tip in a complex tangle thus making the motion of subsequently emits dislocations difficult. The crack remains stationary for a while and then emitted dislocation of a different Burger vector on an inclined slip plane. After a number of dislocations are emitted, the crack turns and propagates along this second slip direction [19].

Zhang and Li[33] clarified the confusion in the literature about the interaction between a screw dislocation and a finite crack. It makes a difference whether a the dislocation is emitted from the crack or comes from else where. For example, both the image force and the shielding effect are always larger for a dislocation emitted from the crack than for the same dislocation originating elsewhere. They become equal if the crack is very long (semi-infinite).

1.3.3 DISLOCATION SHIELDING OF A CRACK TIP:

In addition to dislocation emission at the crack tip, dislocations also play an important role in material toughness through their strong elastic interaction with cracks. when a dislocation is emitted from a crack tip it moves away from the crack tip because the net force on it is positive[32]. The force, however, decreases as inverse square root of distance from crack tip ($\frac{1}{\sqrt{r}}$) and the dislocation comes to rest where the crack force is balanced by the lattice frictional force. The frictional force which is termed as the deformation resistance, is usually a

fraction(<1) of the flow stress of the materials[50]. The region between the crack tip and the area where the dislocation comes to rest is dislocation free and thus the physical origin of the DFZ. The presence of a dislocation in the vicinity of a crack tip modifies the stress field of the region because the interaction between the crack and the dislocation. This phenomenon is very similar to that of work hardening in plastic deformation. During plastic deformation, a dislocation generated from a source exerts back stress on the source. Due to back stress, the stress at the source is reduced accordingly. In order to operate the source and hence to continue deformation, the applied stress must be raised.This increase in the applied stress is one of the causes of work hardening observed during plastic deformation.

The stress field in the immediate vicinity of the crack tip is reduced in the presence of dislocations[31]. this decrease in the stress field reduces the local stress intensity factor K, which is less than the applied stress intensity factor [30]. This reduction in the local stress intensity factor caused by the presence of a dislocation is referred to as dislocation shielding of the crack tip.

1.3.4 CRACK TIP BLUNTING:

After Kelly *et al.*[29] it is generally believed that whether a solid is ductile or brittle depends upon whether the ratio σ_{max}/τ_{max} is large or small. Here σ_{max} is its theoretical tensile strength and τ_{max} is its theoretical shear strength. If this ratio is indeed a critical material constant that determines to a large extent the ductility of a solid, then an atomically sharp crack might be expected to be more easily blunted the larger

is this ratio. When the ratio σ_{max}/τ_{max} is equal to or larger than about seven a mode I crack tip should blunt before brittle crack propagation occurs. The fcc metals satisfy this condition. The bcc metals Iron and Tungsten have σ_{max}/τ_{max} ratio smaller than seven and thus cracks in these metals not blunt.

Weertman[28] used a smeared-out dislocation type analysis to determine condition for the blunting of an atomically sharp crack that is open in tension. When the ratio of the theoretical tensile strength σ_{max} to theoretical shear strength τ_{max} is large, pairs of dislocation of opposite sign are created on an inclined slip plane whose intersection with the crack plane coincides with the crack tip. Dislocation of one sign move into the lattice away from the crack tip region and dislocations of other sign pile-up against the crack tip (*see Fig.* 1.1a). The barrier to the pile-up is the surface energy of the new surface that created during blunting. If the stress is raised further, enough piled up dislocations are created to enable the surface energy barrier to be penetrated. The piled up dislocations enter the crack tip and in doing so blunt the tip(*see Fig.* 1.1b). Weertman concluded that perfect dislocations are not emitted directly from the crack tip as assumed by Rice and Thompson[2], they assumed that a perfect dislocation is emitted directly from the tip itself onto an inclined slip plane. The dislocation move away from the tip, as shown in Fig.(1.1c) and blunt the crack.

The effect of impurity atoms in the crystal lattice, the pinning effect of impurity atoms make it more difficult for a dislocation to move into the lattice away from a crack tip, the qualitative effect of impurity atoms is to make it more difficult

for a crack to be blunted. Impurity atoms in an atmosphere that can the crack surface would decrease the surface energy of solid and thus decrease the ratio σ_{max}/τ_{max}. This effect also makes brittle propagation of a crack more likely.

1.4 POINT DEFECT INTERACTION:

The interaction between second phase particles or point defects with crack and dislocations arises due to misfit stress field present around the second phase particles. The misfit stress result from the second phase particle not exactly fitting into the hole in which it sits. For a spherical inclusion Motto and Nabarro[27] showed that such stresses are proportional to the volume of the second phase particle and decay as the inverse cube of the distance from the second phase particle. The distortions produced around the spherical inclusion are spherically symmetric and only normal stress and strain field are present .

1.4.1 DISLOCATION-POINT DEFECT INTERACTION:

The hydrostatic stress field associated with an edge dislocation can directly interact with an inclusion producing spherically symmetric distortions[44]. Whereas this interaction dose not exist in the case of screw dislocation because of the non-existence of normal stress components, as they can provides a strong interaction if the distortions around inclusion are asymmetric[51]. The interaction between a dislocations and a second phase particle has three distinct contributions, arising from:

(i) Mismatch in elastic constants between matrix and second phase particle.

(ii) Stresses resulting from misfit, and

(iii) The concentration of applied stress by the second phase particle.

If $\frac{\mu}{G} > 1$, the dislocation is repelled from the second phase particle and if $\frac{\mu}{G} < 1$, the interaction is attractive, where μ and G is the shear modulus of inclusion and matrix, respectively. The interaction between moving dislocations and inclusions, may result either in the formation of a dislocation loop around the inclusion or cutting through the inclusion depending on the characteristics of the particle. For hard inclusions, formation of dislocation loops are most likely and for soft inclusions, dislocation cuts through the inclusion causing slip.

1.4.2 CRACK-POINT DEFECT INTERACTION:

There are a number of ways in which a point defect interacts with a crack: a first order size effect arises from interaction between the stress field of the crack tip and the atomic displacement around the point defect. There will also be a second order size effect due to non-linear strains in the vicinity of the crack tip and the importance of this interaction will depend on the magnitude of the third order elastic constants[55]. Since in elastic theory we represent a point defect by an elastic inclusion there will an induced inhomogeneity interaction due to the fact that the material in the inclusion responds to crack tip field under a different Hooke's law from the surrounding material. Liu[26] had discussed the strain field interaction between a crack, loaded in tension and a point defect. This interaction is of importance since the gradient of the interaction energy provides the driving force for the drift flow of point defects to the crack tip. Eshelby[37] had shown that the second order

inhomogeneity effect attracts soft inclusion to the crack tip but repels the hard inclusions. This is just opposite the to the first order size effect.

The second phase particles located in the near tip field of a propagating crack perturb the crack front, causing a reduction in the stress intensity factor. The reduced intensity depends on the character of the particles and the nature of the crack interaction[54]. Two dominant perturbations exists, termed crack bowing and crack deflection. It is essential to discriminate between crack deflection, which produce a non-planar crack and crack bowing, which produces non-linear crack front[24,25]. Crack bowing results from resistant second phase particles in the path of propagating crack, causing the stress intensity K_I along the bowed segment of the crack to decrease, hence increase toughness of the material. Deflection toughening arises whenever interaction between the crack front and the minor phase produces a non-planar crack, subject to a stress intensity factor lower than that experienced by the corresponding planar crack. The non-planar crack arises from elastic modulus mismatch or misfit strain. The sign of misfit strains determines the direction of deflection[23]. Specifically a second phase particle with a greater elastic modulus than the matrix produces a tangential compressive strain near the particle-matrix interface and divert the crack around particle. If elastic modulus is lower than the matrix, induces tangential tensile strains, causing the crack to deflect towards the particle.

CHAPTER 2

2.1 INTERACTION BETWEEN A MOVING CRACK AND DISLOCATION:

Suppose that a mode I crack is extending in a homogeneous and isotropic elastic body in such a way that the state of deformation is two-dimensional plane strain. A rectangular (x,y,z) coordinate system is introduced so that the crack edge is parallel to the z-axis and the displacement vector of each particle is parallel to the x,y-plane, as shown in Fig.(2.1). The crack grows in the x-direction with a uniform velocity å, so that the coordinates of the crack tip in the x,y-plane are x=a(t), y=0, where 'a' is a continuous function of time. The crack tip speed is restricted to the range $0 < å < c_2$ and to be continuous. Two types of waves are originated from the crack tip[38]:

(i) The dilatational wave with the characteristic wave speed c_1.

(ii) The shear wave with the characteristic wave speed c_2.

The dilatational and shear wave speeds for an isotropic elastic material are defined in terms of the mass density ρ and the shear modulus G and Poisson's ratio ν The relationships are [39]:

$$c_1 = \left[\frac{2G}{\rho}\,\frac{1-\nu}{1-2\nu}\right]^{1/2} \qquad (2.1.1)$$

$$c_2 = \left[\frac{G}{\rho}\right]^{1/2} \qquad (2.1.2)$$

The two types of waves are independent in the interior of a solid. At boundaries such as the faces of a crack for example the two types of waves interact.

2.1.1 MOVING CRACK TIP STRESS COMPONENTS:

The x and y axes are fixed in space, so that within the small displacement assumption, a local rectangular coordinate

system ξ and ζ_i (i=1 or 2) are considered at the crack tip. In terms of the position x=a(t) and the speed $\dot{a}$ of the crack tip, the position with respect to local coordinate system is given by the following relations :

$$\xi = x - a(t)$$

and,

$$\zeta_i = \delta_i y \qquad i=1,2$$

Where,

$$\delta_1 = \left[1 - \left(\frac{\dot{a}}{c_1}\right)^2\right]^{1/2}$$

$$\delta_2 = \left[1 - \left(\frac{\dot{a}}{c_2}\right)^2\right]^{1/2} \qquad (2.1.3)$$

A local polar coordinate system (r,θ) is also introduced, where

$$r_i = \sqrt{(\xi^2 + \zeta_i^2)}$$

and, (2.1.4)

$$\theta_i = \tan^{-1}\left[\frac{\zeta_i}{\xi}\right]$$

Using relation (2.1.3), the equation (2.1.4) reduce to the following form :

$$r_i = r\left[1 - (1 - \delta_i^2)\sin^2\theta\right]^{1/2}$$

$$\tan\theta_i = \delta_i \tan\theta \qquad (2.1.5)$$

For a detailed solution see appendix(A).

For a state of steady growth, the crack tip stress field is given by the following equations [39] :

$$\sigma_{ij} = \frac{K_I}{\sqrt{(2\pi r)}} f_{ij}(\theta,\dot{a}) \qquad (2.1.6)$$

Where K_I is stress intensity factor. The function $f_{ij}(\theta,\dot{a})$ represents the angular variation of stress components for any value of crack tip speed $\dot{a}$ and are given below :

$$f_{11} = \frac{1}{D}\left[\left(1+\delta_2^2\right)\left(1+2\delta_1^2-\delta_2^2\right)\frac{\cos(\theta_1/2)}{\sqrt{\gamma_1}} - 4\delta_1\delta_2\frac{\cos(\theta_2/2)}{\sqrt{\gamma_2}}\right]$$

$$f_{22} = -\frac{1}{D}\left[\left(1+\delta_2^2\right)^2\frac{\cos(\theta_1/2)}{\sqrt{\gamma_1}} - 4\delta_1\delta_2\frac{\cos(\theta_2/2)}{\sqrt{\gamma_2}}\right]$$

$$f_{12} = \frac{2\left(1+\delta_2^2\right)}{D}\left[\frac{\sin(\theta_1/2)}{\sqrt{\gamma_1}} - \frac{\sin(\theta_2/2)}{\sqrt{\gamma_2}}\right]$$

$$f_{33} = \nu\,(f_{11} + f_{22}) \qquad (2.1.7)$$

Where ,

$$D = 4\,\delta_1\delta_2 - \left(1+\delta_2^2\right)^2 \qquad (2.1.8)$$

$$\gamma_i = \left[1 - (1-\delta_i^2)\sin^2\theta\right]^{1/2} \qquad (2.1.9)$$

The components of stress have an inverse square root dependence on radial distance from crack tip and a characteristic variation with angular position around the of the crack for crack tip speed in the range $o < \dot{a} < c_2$. In equation (2.1.8), $D \to o$ as $\dot{a} \to c_R$, where c_R is the Rayleigh wave speed. Due to the appearance of the factor D in the expressions for these fields, however, the algebraic sign of the square root singularity depends on whether the crack tip speed is less than or greater than the Rayleigh wave speed of the material c_R. The crack faces separate behind the advancing crack tip and eqns(2.1.7) shows that the stress components have two-fold symmetry and the traction on the prospective fracture plane ahead of the tip is tensile if $o < \dot{a} < c_R$ but that it is compressive if $c_R < \dot{a} < c_2$. This feature implies that there is a net flux of energy out of the advancing crack tip for $c_R < \dot{a} < c_2$, where as there is a net flux of energy into the crack tip for crack tip speed less than the Rayleigh wave speed c_R

2.1.2 STATIONARY CRACK TIP STRESS COMPONENTS:

It can be verified that the equations(2.1.7) do indeed reduce to the equivalent results for a stationary crack in the limit å→o. Irwin-Williams stress fields for a stationary crack[41]:

$$\sigma_{ij} = \frac{K_I}{\sqrt{(2\pi r)}} f_{ij}(\theta) \qquad (2.1.10)$$

Where ,

$$f_{11}(\theta) = \cos(\theta/2)\left[1 - \sin(\theta/2)\sin(3\theta/2)\right]$$

$$f_{22}(\theta) = \cos(\theta/2)\left[1 + \sin(\theta/2)\sin(3\theta/2)\right]$$

$$f_{33}(\theta) = \nu\left[f_{11}(\theta) + f_{22}(\theta)\right]$$

$$f_{12}(\theta) = \cos(\theta/2)\sin(\theta/2)\cos(3\theta/2) \qquad (2.1.11)$$

Some care however is required in arriving at the equations(2.1.11) from eqns(2.1.7) as å → o (see appendix B).

2.1.3 STRESS FIELDS OUTSIDE A SPHERICAL INCLUSION:

Common Inclusions such as Al_2O_3, MnO and SiO_2 are present in many structural materials as they get introduced during manufacturing. These inclusions act as sites for nucleation of defects like cracks and voids and affect the ductile brittle fracture characteristics. Inclusions located in the near tip field of a propagating crack perturb the crack front, causing a reduction in the stress intensity factor.Two dominant perturbations exist, crack bowing and crack deflection as reported by [42]. The stress components are obtained by assuming that a spherical inclusion of radius r° occupies an interstitial site of radius r◦ in an original lattice and distortions produced around the inclusion are spherically symmetric and only normal stress and strain components are presents. Eshelby [43] had given the

outside stress fields around an isotropic inclusion in an isotropic medium as:

$$\sigma_{rr} = -2\sigma_{\psi\psi} = -2\sigma_{\phi\phi} = \frac{8\mu}{3}\left(\frac{1+\nu}{1-\nu}\right)\left(\frac{r^*}{r}\right)^3 \varepsilon$$

$$\varepsilon_{rr} = -2\varepsilon_{\psi\psi} = -2\varepsilon_{\phi\phi} = \frac{1}{3}\left(\frac{1+\nu}{1-\nu}\right)\left(\frac{r^*}{r}\right)^3 \varepsilon \qquad (2.1.12)$$

Where ,

$$\varepsilon = \frac{r^* - r'}{r'} \qquad (2.1.13)$$

The above relation shows that stresses are proportional to the volume of the inclusion and decay as the inverse cube of the distance from the center of the inclusion.

2.1.4 FORCE ON A DISLOCATION:

The crack-dislocation geometry considered to examine force on the dislocation is shown in Fig.(2.2). The slip plane intersects the crack plane at an angle θ along the crack front.The dislocation is parallel to the crack front and thus the geometry is appropriate for treating a dislocation that is emitted from or absorbed at the crack tip. The force on the dislocation is composed of three terms:

1) The force on the dislocation due to the crack stresses.
2) The image force on the dislocation from the crack surfaces, and
3) The interaction between these dislocations and other dislocations present in the matrix.

The image force and the interaction between the dislocation and other dislocations are negligible in comparison to the dominant crack-dislocation interaction. The image force which is always

attractive, however, responsible for the formation of the dislocation-free zone(DFZ) near the crack tip and is inversely proportional to dislocation distance from the crack tip [32].

The transformed crack stresses, σ'_{12}, acting on the slip plane of dislocation obtained by using the following rotation matrix:

$$\begin{bmatrix} \cos\theta & \sin\theta & 0 \\ -\sin\theta & \cos\theta & 0 \\ 0 & 0 & 1 \end{bmatrix} \qquad (2.1.14)$$

The components of stress are given by:

$$\sigma'_{ij} = \alpha_{ik}\,\alpha_{jl}\,\sigma_{kl} \qquad (2.1.15)$$

Where, σ_{kl} is the crack tip stress components and the direction cosines α are given by (2.1.14) as:

$$\alpha_{11} = \alpha_{22} = \cos\theta$$
$$\alpha_{12} = -\alpha_{21} = \sin\theta \quad \alpha_{33} = 1$$
$$\alpha_{31} = \alpha_{13} = \alpha_{23} = \alpha_{32} = 0 \qquad (2.1.16)$$

The resolved shear stress σ'_{12} acting on the slip plane,

$$\sigma'_{12} = \alpha_{1k}\,\alpha_{2l}\,\sigma_{kl}$$
$$= \alpha_{11}[\alpha_{21}\sigma_{11} + \alpha_{22}\sigma_{12} + \alpha_{23}\sigma_{13}] + \alpha_{12}[\alpha_{21}\sigma_{21} + \alpha_{22}\sigma_{22} + \alpha_{23}\sigma_{23}]$$
$$+ \alpha_{13}[\alpha_{21}\sigma_{31} + \alpha_{22}\sigma_{32} + \alpha_{23}\sigma_{33}]$$

Using (2.1.16), σ'_{12} becomes

$$\sigma'_{12} = \cos 2\theta\ \sigma_{12} + \frac{1}{2}\sin 2\theta\ (\sigma_{22} - \sigma_{11}) \qquad (2.1.17)$$

For stationary crack, using (2.1.9) and (2.1.10), σ'_{12} becomes

$$\sigma'_{12} = \frac{K_I}{2\sqrt{2\pi r}}\sin\theta\cos(\theta/2) \qquad (2.1.18)$$

For moving crack, using (2.1.6) and (2.1.7), σ'_{12} becomes

$$\sigma'_{12} = \frac{K_I}{\sqrt{2\pi r}}\left[\cos 2\theta\ f_{12} + \frac{1}{2}\sin 2\theta\ (f_{22} - f_{11})\right] \qquad (2.1.19)$$

The glide force on an edge dislocation that lie on a

slip plane, slip plane intersect the moving crack front, is given by following relation:

$$F = \sigma'_{12}\, b \qquad (2.1.20)$$

Where F is the force per unit length of dislocation and b is the Burger vector of dislocation .

2.2 EFFECT OF INCLUSION ON CRACK-DISLOCATION INTERACTION:

First, we separately examine the interaction between the crack and dislocation and dislocation and inclusion and then by taking all the three crack, dislocation and inclusion together.

2.2.1 CRACK-INCLUSION INTERACTION:

As a first approximation, we treat inclusion as a spherical particle that fits into an undersized or oversized hole, resulting in spherically symmetric normal stresses. Such type of particles interact strongly with the hydrostatic stress at the crack tip (see Fig.2.3).

The hydrostatic stress at the crack tip is given by the relation:

$$-\frac{1}{3}\sum_{i=1}^{3}\sigma_{ij}$$

Following Cottrell's calculation[44] one obtains the elastic interaction:

$$-\frac{1}{3}\sum_{i=1}^{3}\sigma_{ij}\,.\,\Delta V \qquad (2.2.1)$$

Where $\Delta V = 4\pi\varepsilon\, r'^{3}$ is the volume change of the spherical hole.

For moving crack, using (2.1.6) and (2.1.7), the elastic interaction energy Um given by following relation:

$$Um = -\frac{8\pi\, K_I\, (1+\nu)\, \varepsilon\, r'^{3}}{3D\,\sqrt{2\pi r}\,\sqrt{\gamma_1}}\left(1+\delta_2^2\right)\left(\delta_1^2-\delta_2^2\right)\cos(\theta_1/2) \qquad (2.2.2)$$

$$Um = -\frac{M\, K_I}{D\,\sqrt{r\gamma_1}}\left(1+\delta_2^2\right)\left(\delta_1^2-\delta_2^2\right)\cos(\theta_1/2) \qquad (2.2.3)$$

Similarly, for stationary crack, using(2.1.9) and (2.1.10), the elastic interaction energy Us are :

$$Us = - \frac{8\pi . K_I . (1+\nu) . \varepsilon . r'^{3}}{3\sqrt{2\pi r}} \cos(\theta/2) \qquad (2.2.4)$$

$$Us = - \frac{M K_I}{\sqrt{r}} \cos(\theta/2) \qquad (2.2.5)$$

Where, $M = \frac{8\pi . (1+\nu) . \varepsilon . r'^{3}}{3\sqrt{2\pi}}$ is a constant.

The equipotential curve for moving and stationary crack have been drawn in Fig.(2.3) and Fig.(2.4), using (2.2.3) and (2.2.5) respectively. The equipotential curves are the contours having constant values of

$$\frac{1}{D\sqrt{r\gamma_1}} \left(1 + \delta_2^2\right)\left(\delta_1^2 - \delta_2^2\right).\cos(\theta_1/2)$$

for moving crack, for different normalized crack tip speed. For a stationary crack, the contours have constant values of $r^{-1/2}\cos\theta$. The negative of first derivative of interaction energy($-\frac{\partial U}{\partial r}$) gives the force on the inclusion. This force is attractive if ε is positive and repulsive if ε is negative.

2.2.2 DISLOCATION-INCLUSION INTERACTION:

For the case of a straight positive edge dislocation in elastically isotropic materials, the stresses in terms of the three orthogonal coordinate axes, are given by the following equations [45]:

$$\sigma^{d'}_{11} = - to \frac{b \sin\theta \,(2\cos^2\theta + 1)}{r}$$

$$\sigma^{d'}_{22} = to \frac{b \sin\theta \cos 2\theta}{r}$$

$$\sigma^{d'}_{33} = - to \frac{2 b \nu \sin\theta}{r}$$

$$\sigma^{d'}_{12} = to \frac{b \cos\theta \cos 2\theta}{r} \qquad (2.2.6)$$

Where, $to = \frac{G}{2\pi (1-\nu)}$

The hydrostatic stress of a positive edge dislocation at position (r,θ) (Fig.(2.5)) from the dislocation is

$$\sigma_m = -\frac{1}{3}\left(\sigma^{d'}_{11} + \sigma^{d'}_{22} + \sigma^{d'}_{33}\right)$$

$$= \frac{(1+\nu)\, G\, b \sin\theta}{3\pi\,(1-\nu)\, r} \qquad (2.2.7)$$

Here, again the inclusion is treated as a point defect causing spherically symmetric distortions. Hence the interaction only occurs with the hydrostatic component of the dislocation stress field. The elastic interaction energy between the dislocation and the inclusion is obtain using (2.2.1):

$$Ui = \frac{4\,(1+\nu)\, G\, b\, r'^3 \varepsilon \sin\theta}{3\pi\,(1-\nu)\, r}$$

$$Ui = A\frac{\sin\theta}{r}\,\varepsilon \qquad (2.2.8)$$

Where,

$$A = \frac{4\,(1+\nu)\, G\, b\, r'^3}{3\pi\,(1-\nu)}$$

Note: In section (2.2.1) and (2.2.2), the interaction energy includes only the energy external to the inclusion. It neglects the strain energy change within the inclusion. If the energy change of the inclusion is included, the interaction energy is modified by a constant factor[46].

2.2.3 CRACK-DISLOCATION-INCLUSION SYSTEM:

The geometric configuration used in our calculations is shown in Fig.(2.6). We assume that the nature of each source of stress is unaffected by the presence of the others. So that we can superimpose, stresses from different sources over each other. The total shear stress experienced by the dislocation is obtained by the algebraic summation of stresses from the individual sources, *i e.* the crack and the inclusion.

The dislocation and the inclusion are taken in the same orthogonal coordinate system(x',y',z'). The shear stress on the dislocation due to the inclusion is obtained by using the

following transformation matrix:

$$\begin{bmatrix} \sin\phi\cos\psi & -\sin\psi\cos\phi & \cos\psi \\ \sin\phi\sin\psi & \cos\psi\cos\phi & \sin\psi \\ \cos\phi & 0 & -\sin\phi \end{bmatrix} \qquad (2.2.9)$$

Using eqns(2.1.11) and (2.1.14), one obtained the σ^{I}_{12} for inclusion as below:

$$\sigma^{I}_{12} = \alpha_{11}\alpha_{21}\sigma_{rr} + \alpha_{12}\alpha_{22}\sigma_{\psi\psi} + \alpha_{13}\alpha_{23}\sigma_{\phi\phi} \qquad (2.2.10)$$

Using(2.2.9), (2.2.10) becomes on simplification:

$$\sigma^{I}_{12} = 2\mu\left(\frac{1+\nu}{1-\nu}\right)\left(\frac{r^{*}}{r}\right)^{3}\varepsilon \sin 2\psi \sin^{2}\phi \qquad (2.2.11)$$

Now, total resolved shear stress on dislocation, obtained by using (2.2.11) and (2.1.17), for stationary crack:

$$\sigma^{T,s}_{12} = \sigma^{'s}_{12} \pm \sigma^{I}_{12} \qquad (2.2.12)$$

and, for moving crack, using (2.2.11) and (2.1.18) :

$$\sigma^{T,m}_{12} = \sigma^{'m}_{12} \pm \sigma^{I}_{12} \qquad (2.2.13)$$

Here superscripts 's' and 'm' refer to stationary and moving crack, respectively. The ± sign put because ε may be positive or negative.

The force on dislocation, per unit length of dislocation is given by :

$$F = \sigma^{T}_{12}.\, b \qquad (2.2.14)$$

For a typical value of $r^{*}/r = 0.8$, $\varepsilon = +0.55\times10^{-2}$ and μ = 156Gpa for Al_2O_3 in Fe matrix [47] and $\nu = 0.33$, K_I = 65Mpa$\sqrt{m}$, r = 10μm and G = 736pa for Fe, the force on dislocation have been calculated for different normalized crack tip velocity and plotted in Fig.(2.6).

2.3 STRAIN ENERGY AND INTERACTION ENERGY OF CRACK, DISLOCATION AND INCLUSION SYSTEM:

2.3.1 STRAIN ENERGY OF A CRACK:

The extension of crack requires the formation of a new surface, with its associated surface energy. The elastic strain energy density stored in the body is released in the process of generation of new surface. The strain energy density is given by:

$$U_c = \frac{1}{2}\,\sigma_{ij}\,\varepsilon_{ij} \qquad (2.3.1)$$

Where,

$$\varepsilon_{ij} = \frac{1+\nu}{E}\,\sigma_{ij} - \frac{\nu}{E}\,\sigma_{kk}\,\delta ij$$

$$\delta_{ij} = 1 \quad \text{when } i=j$$

$$= 0 \quad \text{when } i\neq j \qquad (2.3.2)$$

For mode I loading, using relation (2.3.2) and (2.3.1):

$$U_c = \frac{1}{2E}\left(\sigma_{11}^2+\sigma_{22}^2+\sigma_{33}^2\right) - \frac{\nu}{E}\left(\sigma_{11}\sigma_{22}+\sigma_{22}\sigma_{33}+\sigma_{33}\sigma_{11}\right) + \frac{1}{2G}\sigma_{12}^2$$

Now, for a moving crack using relation (2.1.6) and (2.1.7), the above relation becomes:

$$U_c^m = \frac{K_I^2}{2\pi r}\left[\frac{1}{2E}\left(f_{11}^2+f_{22}^2+f_{33}^2\right) - \frac{\nu}{E}\left(f_{11}f_{22}+f_{22}f_{33}+f_{33}f_{11}\right) + \frac{1}{2G}f_{12}^2\right]$$

$$U_c^m = f(r).f(\theta,\dot{a}) \qquad (2.3.3)$$

Where,

$$f(r) = \frac{K_I^2}{2\pi r}$$

$$f(\theta,\dot{a}) = \frac{1}{2E}\left(f_{11}^2+f_{22}^2+f_{33}^2\right) - \frac{\nu}{E}\left(f_{11}f_{22}+f_{22}f_{33}+f_{33}f_{11}\right)+\frac{1}{2G}f_{12}^2$$

Here, f(r) is a function of radial distance 'r' and $f(\theta,)$ is a function of angular displacement θ and crack tip velocity '$\dot{a}$'. Similarly, for a stationary crack using relation (2.1.9) and (2.1.10), strain energy density is given by the relation :

$$U_c^s = f(r).f(\theta) \qquad (2.3.4)$$

Where,

$$f(r) = \frac{K_I^2}{2\pi r}$$

$$f(\theta) = \frac{1}{2E}\left(f_{11}^2(\theta) + f_{22}^2(\theta) + f_{33}^2(\theta)\right) - \frac{\nu}{E}\left(f_{11}(\theta)f_{22}(\theta) + f_{22}(\theta)f_{33}(\theta) + f_{33}(\theta)f_{11}(\theta)\right) + \frac{1}{2G}f_{12}^2(\theta)$$

The angular variation of strain energy density for moving and static crack have been plotted in Fig.(2.7).

For the volume element r $d\theta$ dr dz, the total strain energy per unit length of crack front is given by the relation:

$$E_c = \int_0^{2\pi} \int_{R^*}^{R} U_c \; r \; d\theta \, dr \qquad (2.3.5)$$

Since there is a singularity at crack tip, the lower limit is taken as some finite small value R^*.

For moving crack, using (2.3.5) and (2.3.3), we get

$$E_c^m = \frac{K_I^2(R - R^*)}{2\pi} \int_0^{2\pi} f(\theta,\dot{a}) \; d\theta \qquad (2.3.6)$$

Similarly, for stationary crack, using (2.3.4), we get

$$E_c^s = \frac{K_I^2(R - R^*)}{2\pi} \int_0^{2\pi} f(\theta) \; d\theta \qquad (2.3.7)$$

The integral (2.3.6) and (2.3.7) have been solved with the help of Simpson's three point numerical integration formula. Numerical results have been plotted for different crack tip velocity in Fig.(2.8).

2.3.2 STRAIN ENERGY OF AN STATIC EDGE DISLOCATION:

The total strain energy of a dislocation is the sum of the elastic strain energy plus the energy of the core of the dislocation. As a good approximation, the core energy is added to the elastic strain energy by taking core radius $r_o = b$, so that the total strain energy per unit length of edge dislocation is given by[45]:

$$U = \frac{G\,b^2}{4\,\pi\,(1-\nu)} \ln\frac{r}{b} \qquad (2.3.8)$$

2.3.3 STRAIN ENERGY DENSITY OF A MOVING DISLOCATION:

We consider a subsonic discrete dislocation in uniform motion in an isotropic media. The moving straight dislocation is considered to remain straight during motion referred to its own cartesian frame and lies parallel to the z-axis and moves in the x-direction with velocity υ within the subsonic velocity range $0 < \upsilon < c_2$. The dislocation source producing the dislocation lies on the slip plane that intersects the crack front. Let the source produce an equal number of positive and negative edge dislocations at any time as a result of the moving crack stresses. The total number n of dislocations matching the crack strain energy density to that of a giant dislocation of Burger vector nb required to replace the moving crack stress fields on the slip plane of dislocation. The stress field is then obtained by considering a giant dislocation of Burgers vector nb present on the slip plane as shown in Fig.(2.15) at all instant of crack motion and then breaking down to n elementary dislocations after the passage of the crack. The stress field associated with a uniformly moving edge dislocation of Burgers vector b is given by the following relations[43]:

$$p_{11} = \frac{2\,G\,b\,c_2^2\,\sin\beta}{\pi\,\upsilon^2\,d}\left[-\frac{\delta_3\,(\delta_4^2 + 1 - \omega^2)}{\cos^2\beta + \delta_3^2\sin^2\beta} + \frac{\omega^2\,\delta_4}{\cos^2\beta + \delta_4^2\sin^2\beta}\right]$$

$$p_{22} = \frac{2\,G\,b\,c_2^2\,\sin\beta\,\omega^2}{\pi\,\upsilon^2\,d}\left[\frac{\delta_3}{\cos^2\beta + \delta_3^2\sin^2\beta} - \frac{\delta_4}{\cos^2\beta + \delta_4^2\sin^2\beta}\right]$$

$$p_{12} = \frac{2\,G\,b\,c_2^2\,\cos\beta}{\pi\,\upsilon^2\,d\,\delta_4}\left[\frac{\delta_3\,\delta_4}{\cos^2\beta + \delta_3^2\sin^2\beta} - \frac{\omega^4}{\cos^2\beta + \delta_4^2\sin^2\beta}\right]$$

$$P_{33} = \nu\left(P_{11} + P_{22}\right) \qquad (2.3.9)$$

Where, $\omega = \left[1 - \frac{v^2}{2\,c_2^2}\right]^{1/2}$

$$\delta_3 = \left[1 - \left(\frac{v}{c_1}\right)^2\right]^{1/2} \quad ; \quad \delta_4 = \left[1 - \left(\frac{v}{c_2}\right)^2\right]^{1/2}$$

The strain energy of a dislocation is proportional to the square of the Burbers vector of the dislocation. The total strain energy of the giant dislocation of Burger vector nb is going to be considerably greater than the sum of the strain energy of n dislocations of Burgers vector b because

$$(nb)^2 >> n \sum b_i^2$$

Where $b_i = b$, is the Burgers vector of the elementary dislocation. Hence a giant dislocation of Burgers vector nb could burst into n component dislocations each with Burgers vector b, followed by an overall reduction in the energy of the system when the crack has passed through an active slip plane. The total number of dislocations in the pileup is given by the relation[51]:

$$n\,\alpha = \frac{r\,\sigma'_{12}}{G\,b} \qquad (2.3.10)$$

Where, α is a correction factor for the case of dynamic dislocations and moving cracks.

Using eqns(2.3.1) and (2.3.2), the strain energy density of the moving dislocation is given by the relation:

$$U_d^m = \frac{1}{2E}\left(P_{11}^2 + P_{22}^2 + P_{33}^2\right) - \frac{\nu}{E}\left(P_{11}\,P_{22} + P_{22}\,P_{33} + P_{33}\,P_{11}\right) + \frac{1}{2G}P_{12}^2 \qquad (2.3.11)$$

The plots of eqn(2.3.11) are shown in Fig.(2.9) for different normalized dislocation velocity.

2.3.4 STRAIN ENERGY OF AN INCLUSION:

If a matrix volume is filled with a spherical inclusion of radius(r^*) and the body forces removed, then the matrix will relax, and the stress and strain fields produced are given by eqn(2.1.11). The strain energy stored in the inclusion is given by[56]:

$$U_I = \frac{1}{2} \sigma_{rr} . \Delta v \qquad (2.3.12)$$

Where Δv is the change in volume of the inclusion and equals to $4\pi\varepsilon r'^3$. Using eqn(2.1.11), eqn(2.3.12) becomes

$$U_I = \frac{16\pi\mu}{3} \left(\frac{1+\nu}{1-\nu}\right) \varepsilon^2 \frac{r^{*d}}{r^s} \qquad (2.3.13)$$

2.3.5 INTERACTION ENERGY BETWEEN CRACK AND DISLOCATION:

The interaction energy between a crack and dislocation is taken as the average of crack to dislocation energy (Ec → d) and dislocation to crack interaction energy (Ed → c) per unit length of crack front:

$$Ec - d = \frac{1}{2} \left[Ec \rightarrow d + Ed \rightarrow c \right] \qquad (2.3.14)$$

The subscripts 'c' and 'd' refer to crack and dislocation, respectively. For volume element r dθ dr dz, interaction energy Ed → c per unit length of crack front is given by following relation:

$$Ed \rightarrow c = \int_0^{2\pi} \int_{r^*}^{r} \left(\sigma_{ij}^d \varepsilon_{ij}^c \right) r \, dr \, d\theta \qquad (2.3.15)$$

The σ_{ij}^d is the dislocation stress components at crack tip, which is obtained by using the transpose of the rotation matrix (2.1.14) and relation (2.1.15) and (2.2.6). The relations are :

$$\sigma_{11}^d = \cos^2\theta \, \sigma_{11}^{d'} + \sin^2\theta \, \sigma_{22}^{d'} - \sin 2\theta \, \sigma_{12}^{d'}$$

$$\sigma_{22}^d = \sin^2\theta \, \sigma_{11}^{d'} + \cos^2\theta \, \sigma_{22}^{d'} + \sin 2\theta \, \sigma_{12}^{d'}$$

$$\sigma_{33}^d = \nu \left(\sigma_{11}^{d'} + \sigma_{22}^{d'} \right)$$

$$\sigma^{d}_{12} = \frac{1}{2}\sin 2\theta\left(\sigma^{d'}_{11} - \sigma^{d'}_{22}\right) + \cos 2\theta\ \sigma^{d'}_{12} \qquad (2.3.16)$$

For a moving crack using eqns(2.3.2), (2.1.6) and (2.1.7), ε^{c}_{ij} are given by following relations:

$$\varepsilon^{c}_{11} = \frac{K_I}{E\sqrt{2\pi r}}\left[f_{11} - \nu\left(f_{22} + f_{33}\right)\right]$$
$$\varepsilon^{c}_{22} = \frac{K_I}{E\sqrt{2\pi r}}\left[f_{22} - \nu\left(f_{11} + f_{33}\right)\right]$$
$$\varepsilon^{c}_{22} = 0$$
$$\varepsilon^{c}_{12} = \frac{1+\nu}{E}\ \frac{K_I}{\sqrt{2\pi r}}\ f_{12} \qquad (2.3.17)$$

Similarly for stationary crack, using eqns(2.3.2), (2.1.9) and (2.1.10), ε^{c}_{ij} are given by following relations :

$$\varepsilon^{c}_{11} = \frac{K_I}{E\sqrt{2\pi r}}\left[f_{11}(\theta) - \nu\ \left(f_{22}(\theta) + f_{33}(\theta)\right)\right]$$
$$\varepsilon^{c}_{22} = \frac{K_I}{E\sqrt{2\pi r}}\left[f_{22}(\theta) - \nu\left(f_{11}(\theta) + f_{33}(\theta)\right)\right]$$
$$\varepsilon^{c}_{33} = 0$$
$$\varepsilon^{c}_{12} = \frac{1 + \nu}{E}\ \frac{K_I}{\sqrt{2\pi r}}\ f_{12}(\theta) \qquad (2.3.18)$$

The σ^{d}_{ij} and ε^{c}_{ij}, both are functions of two independent variables r and θ, hence integral(2.3.15) can be solved for moving and stationary crack separately with the help of Simpson's three point numerical integration formula for different normalized crack tip speed.

Now, the interaction energy Ec → d per unit length of crack front is given by the relation :

$$Ec \rightarrow d = \int_{R}^{r} \sigma^{c'}_{12}.b\ dr \qquad (2.3.19)$$

Where 'R' is the distance from crack tip to the boundary of medium For stationary crack, using eqn(2.1.17) and integrating (2.3.19), it become:

$$Ec \rightarrow d = \frac{K_I\ b\ (\sqrt{r} - \sqrt{R})}{\sqrt{2\pi}}\sin\theta\cos\frac{\theta}{2} \qquad (2.3.20)$$

For moving crack, using eqn(2.1.19) and integrating eqn(2.3.19), it becomes:

$$Ec \rightarrow d = \frac{2 K_I b (\gamma_r - \gamma_k)}{\gamma 2\pi} \left[f_{12} \cos 2\theta + \frac{1}{2} \sin 2\theta \left(f_{22} - f_{11} \right) \right] \qquad (2.3.21)$$

The variation of interaction energy between crack and dislocation with θ and for different normalized crack tip speeds have been shown in Fig.(2.10).

CHAPTER 3

RESULTS AND DISCUSSIONS

3.1 FORCE ON A DISLOCATION:

The Fig.(2.2) shows the variation of force F with θ for static and moving cracks for different normalized crack tip speeds ($\dot{a}/c_2$). The plots have two fold symmetry around the crack edge. For crack speeds less than about twenty percent of the shear wave speed c_2 of the material, the force has a maximum value along $\theta = 70^o$. For crack speeds greater than $0.2c_2$, however, this force has a maximum in a direction perpendicular to the direction of crack motion($\theta = 90^o$). For crack speeds greater than or equal to $0.8c_2$, the curves have two maxima. The first maximum, which is of a greater magnitude, is at $\theta = 90^o$, for all speeds greater than $0.8c_2$. The second smaller maximum has its position along $\theta = 30^o$ at crack speed of $0.8c_2$ and along $\theta = 40^o$ for all speeds in the range $0.90c_2 < \dot{a} < c_R$, c_R is Rayleigh wave velocity and it is approximately equal to $0.93c_2$. Rayleigh waves are characterized as waves which propagate parallel to the surface of a semi-infinite solid and whose amplitude is greatest at the surface and decreases exponentially with distance from the surface. It is neither purely longitudinal nor purely transverse. At the Rayleigh wave velocity the force on the dislocation becomes infinite. In the range $0 < \dot{a} < c_R$, the magnitude of the maximum increases with increasing crack speeds (see figures (2.2a) and (2.2b)). The second smaller maximum has its position along $\theta = 50^o$ for all speeds in the range $c_R < \dot{a} < c_2$, however, the

magnitude of the maximum decreases with increasing crack speeds further (see fig.(2.2c)). The force becomes attractive or repulsive depends on speeds of the crack tip and angular positions of the dislocation. The Table(2.1) shows the nature of the maximum force.

Any emitted dislocation from crack tip or lattice dislocation moves away from crack tip under the repulsive force. However, a dislocation comes to rest at a point on the slip plane where the force on the dislocation is balanced by the lattice frictional force or by any other dislocation barrier such as inclusions. The dislocations pile up at this barrier. The piled-up dislocations exert image forces on the crack tip. The image force is always attractive and inversely proportional to the distance from the crack tip[32]. This image force is responsible for the DFZ near a crack tip[2]. The crack tip shielding provided by piled-up dislocations against applied stresses, reduces the local stress intensity factor at crack tip[30]. The reduction in local stress intensity factor, may delay the crack propagation or the crack may deviate from its original path until piled-up dislocations cross the barrier. In the process the ductile to brittle transition point may shift towards the brittle side for the moment. If the Burgers vector of the emitted dislocation, had a component perpendicular to the crack front, then emitted dislocations blunt the crack tip. The local stress intensity factor also is reduced by blunting. Therefore, it is necessary to increase the shear stress to propagate the crack further. This is in analogy to the work hardening of materials.

In the range $0.9c_t < \dot{a} < c_R$ the lattice dislocations present at slip planes that intersect the crack front move towards the crack tip under the attractive force of crack at orientations such as $\theta = 40^\circ$. With progressive crack growth, the movement of lattice dislocations is accompanied by plastic deformation near the crack tip region. The plastic deformation gives rise to blunting of crack tip and thus hinders the crack propagation. The movement of lattice dislocations at the crack tip during crack growth is therefore important in the case of ductile materials.

3.2 EFFECT OF INCLUSION ON CRACK-DISLOCATION INTERACTION:

3.2.1 CRACK-INCLUSION INTERACTION:

In Fig.(2.3) and Fig.(2.4), the equipotential curves for static and moving cracks have been plotted. The two possible cases $\varepsilon > 0$, and $\varepsilon < 0$ are separately considered.

Case I - If ε is positive, the interaction energy is lowest ahead of a crack tip, *i.e.* $\theta = 0^\circ$, for static as well as moving cracks. In other words, the attractive force on the inclusion is highest ahead of a crack tip, *i e* $\theta = 0^\circ$, for static as well as moving cracks. An inclusion with a greater elastic modulus such as many carbides in α-Fe matrix produces a tangential compressive strain near the inclusion-matrix interface. Hence, under the radial attractive force, a crack could divert itself around the inclusion. For a static crack (Fig.(2.4)), the interaction energy increases from minimum at $\theta = 0^\circ$ to maximum at $\theta = \pi$ for all equipotential curves. For a moving crack(Fig.(2.3)), the equipotential curves have two fold symmetry around the crack tip. The interaction energy increases from minimum at $\theta = 0^\circ$ to maxima

at $\theta = \pi/2$, and again decreases from maximum at $\theta = \pi/2$ to minimum at $\theta = \pi$. For a static crack, the interaction energy is zero for $\theta = \pi$, however, for a moving crack the interaction energy never becomes zero for any angular position.

Case II - If ε is negative, the interaction energy is maximum ahead of the crack tip, *i e* $\theta = 0^{o}$, for a static as well as for a moving crack. In other words, the repulsive force on the inclusion is highest for the position $\theta = 0^{o}$.

3.2.2 DISLOCATION-INCLUSION INTERACTION:

Case I - If ε is positive, the interaction energy is negative for $\pi < \theta < 2\pi$, hence an inclusion will attract a positive edge dislocation with its compression side lying on the side of the inclusion. The most favorable position for inclusion is at $\theta = 3\pi/2$, where the interaction energy is minimum or attractive force is maximum. The inclusion will repel a positive edge dislocation with its tension side being on the inclusion for the positions in between $0 < \theta < \pi$.

Case II - If ε is negative, then from eqn(2.2.12), it is clear that interaction energy is negative for, $0 < \theta < 2\pi$, hence an inclusion causing a negative misfit strain will attract a positive edge dislocation with its tension side lying on the side of the inclusion. The most favorable position for inclusion is at $\theta = \pi/2$, where the interaction energy is minimum or attractive force is maximum. The inclusion will repel a positive edge dislocation with its compression side being on the inclusion for $\pi < \theta < 2\pi$.

3.2.3 CRACK-DISLOCATION-INCLUSION SYSTEM:

The quantitative effect of inclusion on

crack-dislocation interaction is shown in Figures(2.6). The Fig(2.6a) shows the variation of force with θ on the dislocation in the presence of the inclusion. The maximum force acting on the dislocation changes its position to $\theta = 60^{o}$ from $\theta = 70^{o}$ for a static crack. The magnitude of the force is also increased. For the static crack the curves are no more symmetric around the crack. For static crack the maximum in the range $\theta = \pi$ to 2π is at 280^{o}. For speeds in the range $0.2c_{2} < \dot{a} < 0.8c_{2}$, the curves are two fold symmetric around the crack and the magnitude of the force increases for all angular positions. Table(3.2) shows the angular position for the maximum force on the dislocation at different crack speeds and for $\phi = 30^{o}$, 45^{o}, 60^{o}, 70^{o}, taken around the inclusion.

3.3 STRAIN ENERGY DENSITY OF CRACK:

The minimum strain-energy-density criterion(MSED), proposed by Sih[42] postulates that a crack propagates along a direction of minimum elastic strain energy density. Fig.(2.7) shows the variation of the strain energy density U_{c} with θ around a crack for different normalized crack speeds and at a fixed radial distance r from crack tip. For the static crack, the strain energy density increases from zero at $\theta = \pi$ to maximum at $\theta = 70^{o}$ and again to a minimum at $\theta = 0^{o}$. For a moving crack, the strain energy density plots have two fold symmetry around the crack for all speeds. With increasing crack tip speeds, the magnitude of the strain energy density increases for all angular positions. Taking Sih's postulate into consideration it may be concluded from Fig.(2.7) that the likely direction of crack propagation is along

the direction $\theta = 0^{o}$ in the velocity range $0 \leq \dot{a} \leq 0.6c_{2}$. At $\dot{a} = 0.8c_{2}$, curves have minimum strain energy density along the direction $\theta = 60^{o}$, and hence a crack will propagate in this direction. At speeds greater than $0.8c_{2}$, the curves have minimum strain energy density along the direction $\theta = 70^{o}$, and therefore the most likely direction for crack propagation.

Fig.(2.8) shows the variation of total strain energy per unit length of crack front with normalized crack tip speeds. In the speeds $0 < \dot{a} < c_{2}$(fig.(2.8a)), the total strain energy increases continuously and variation is logarithmic in character because there is a net flux of energy into the crack tip. As speeds tend to the Rayleigh wave speed c_{R}, the total strain energy of crack tends to infinity. This indicates that the crack becomes more and more unstable as crack tip speed increases and in the vicinity of Rayleigh wave speed, the crack is most unstable. The possible bifurcation of crack may take place to minimize the energy of the system. The increase instability of the crack with increasing velocity is due to the lower energy release rate from the crack tip. In the speed range $c_{R} < \dot{a} < c_{2}$, the total strain energy of crack decreases with increasing velocity from infinity as shown in fig.(2.8b) because there is a net flux of energy out of the advancing crack tip and decreased instability of the crack.

3.4 STRAIN ENERGY DENSITY OF A MOVING DISLOCATION:

The Fig.(2.9) shows the variation of strain energy density with angle β around a positive edge dislocation for different normalized dislocation velocities for a fixed radial distance r. The plots have two fold symmetry around the

dislocation. For β = 0, the maximum of the strain energy density decreases with increasing velocity of the dislocation up to $0.4c_2$. At v/c_2= 0.6, the plot has maximum strain energy density at β = 40^o and at v/c_2= 0.8, maximum located at $\beta = 60^o$. For $\beta = 90^o$, the strain energy density increases with increasing velocity of the dislocation.

3.5 DISLOCATION GENERATION BY CRACK:

Shear stresses from moving cracks can cause dislocation sources to operate on the slip planes that intersect the crack front. An inclusion present on the slip plane can also act as a source for dislocation loop formation etc., when an emitted dislocation encounters the inclusion and crosses it, leaving behind a dislocation loop around the inclusion. To obtain an equivalent number of dislocations to match the crack shear stress, we equate the strain energy density of a crack at an angular position(r,θ) with the strain energy density of the moving dislocation at an angular position(d,β). As an example, the number of dislocations have been calculated for dislocation velocities in the range $0 < v < 0.9c_2$ at normalized crack tip velocities 0.2, 0.6 and 0.8 and the results are plotted in Fig.(2.11) for $\theta = 70^o$, $\beta = 0^o$, and r = d = 10μm. Fig.(2.11) shows that the number of edge dislocations equivalent to the crack shear stress increases with increasing dislocation velocity and variation is logarithmic in character for all crack velocities. However, with increasing crack velocity, the graphs move upwards. The number of dislocations increases with increasing crack velocity at all dislocation velocities. There is more pronounced

increase in the number of dislocations in the velocity range $0.8c_2 < \dot{a} < c_R$. The graph is restricted to the dislocation velocity less than the Rayleigh velocity c_R and the number of dislocations is of the order 10^4.

Fig.(2.12) shows the distribution of the number of dislocations with normalized dislocation velocity and for different radial distance between crack and source for a fixed crack tip velocity(d = 10μm, r = 5, 10, 20, 30, 50, 100μm, $\theta = 70^o$, $\beta = 0^o$, and $\dot{a} = 0.8c_2$). The graphs moves downwards as the distance r increases. The number of dislocations decreases but the trend of graphs is the same for all radial distances. The Fig.(2.13) shows the distribution of number of dislocation with radial distance r and for $\theta = 70^o$, $\beta = 0^o$, d = 10μm, v/c_2= 0.2, 0.6, 0.8 and $\dot{a} = 0.8c_2$. There is decrease in the number of dislocations with increase in distance. The graphs move upwards as dislocation velocity increases. The Fig.(2.14) shows the distribution of number dislocations with shear stress acting on the dislocation and for $\theta = 70^o$, $\beta = 0^o$, d = 10μm, r = 10μm, and v/c_2= 0.2, 0.6, 0.8. The plot shows the increase in number of dislocations with increase in shear stress as a function of the dislocation velocity. The Fig.(2.16) shows the variation of number of dislocations with $\sigma'_{12}r$ for $\theta = 70^o$, $\beta = 0^o$, d = 10μm, and $v = \dot{a} = 0.8c_2$. The number of dislocations decreases with increasing the quantity $\sigma'_{12}r$ and variation is approximately hyperbolic.

3.6 DISLOCATION SUB-STRUCTURE:

An acting dislocation source producing n number of

dislocations at any time, can have an equal number of positive and negative edge dislocations out of the total number n, with one half moving away from the crack tip under strong repulsive forces of the crack for θ between -5^{o} to 85^{o} and for crack tip speeds in the range $0.2c_{z} \leq \dot{a} \leq 0.6c_{z}$ (see Fig.2.2a). These positive edge dislocations once formed relax into the matrix. The remaining n/z negative edge dislocations move towards the crack tip under strong attractive forces of the crack. This is reversed in the lower of the crack plane for θ between 265^{o}-355^{o} and for crack tip speeds in the range $0.2c_{z} \leq \dot{a} \leq 0.6c_{z}$, the positive edge dislocations move towards the crack tip and negative edge dislocations move away from the crack tip and relax into the matrix. The movement of edge dislocations towards the crack tip results in many sub-structural changes ahead of crack tip and some of the interesting cases are considered in the ongoing discussion.

Case I: Suppose there is no barrier for dislocation movement, except the moving crack surface. The movement of dislocations is accompanied by plastic deformation. As the density of dislocations builds up at the crack tip, the plastic deformation is sufficient to slip or blunt the crack tip. The possible resulting crack geometry is shown in Fig.(2.17). The crack tip stress field promotes the generation of dislocations from a source, since it reduces the back stress on the source by pulling away the dislocations from the source. When blunting occurs, crack relaxes for a moment and then moves forwards. Crack tip blunting reduces the stress intensity factor and this results in slowing down the generation of dislocations at that particular

slip plane containing the dislocation source.

Case II: Suppose there are barriers such as an inclusion in between the crack tip and the dislocation source, where the inclusion is harder than the matrix. The n/z dislocations pile up at the inclusion leading to the possible nucleation and growth of a new crack as shown in Fig.(2.18). Since the edge dislocations cannot climb like screw dislocations, the only option left for dislocations is to relax at the barrier by forming a new crack. The direction of the new crack is approximately at 90^{o} to the slip plane of of dislocations. This case is possible in the case of relatively brittle materials.

Case III: If inclusion is harder and lies in a ductile matrix. The nucleation and growth of voids at the inclusion-matrix interface may be facilitated due to the build up of a tensile hydrostatic stress component from dislocations stresses in an already otherwise tensile field of the crack. The crack attracts the inclusion towards the crack tip and the attractive force on the dislocations also favors the displacement of inclusion towards the crack tip that results in building up of a gap between the inclusion and the matrix surfaces as shown in Fig.(2.19). This gap acts as a nucleation site for void growth. These mechanisms are some of the possibilities in the case of ductile fracture.

CHAPTER 4

SUMMARY AND CONCLUSIONS

1) The shear stress σ'_{12} associated with a moving crack has a different spatial dependence than that of a static crack and has two fold symmetry around the crack tip.

2) For crack speeds less than or equal to $0.2c_2$ an edge dislocation experiences a maximum force on slip plane inclined at $\theta = 70^{\circ}$. For crack speeds in the range $0.2c_2 < \dot{a} < 0.8c_2$, the maximum is along $\theta = 90^{\circ}$. For crack speeds greater than or equal $0.8c_2$, the curves have two maxima. The first maximum of greater magnitude is along $\theta = 90^{\circ}$ for all speeds greater than $0.8c_2$. The second smaller maximum is along $\theta = 30^{\circ}$ for crack speed $0.8c_2$. For crack speeds in the range $0.9c_2 \leq \dot{a} \leq c_R$ second maximum is located in the direction $\theta = 40^{\circ}$. For crack speeds in the range $0 \leq \dot{a} \leq c_R$, the magnitude of force increases with increasing crack speeds for all angular positions. For crack speeds in the range $c_R < \dot{a} < c_2$, the second maximum have position along $\theta = 50^{\circ}$, but magnitude of force decreases with increasing crack speeds above c_R.

3) The force on the dislocation tends to infinity at $c_R \cong 0.93c_2$, where c_R is the Rayleigh wave velocity.

4) An inclusion with a positive misfit strain experiences a maximum attractive force along $\theta = 0^{\circ}$ from a moving as well as a static crack. If the elastic modulus of the inclusion is greater than that of the matrix, diverts the crack around

the inclusion.

5) For a negative misfit strain, inclusion will attract a positive edge dislocation with its tension side lying on the side of the inclusion.

6) For a positive misfit strain, inclusion will attract a positive edge dislocation with its compression side lying on the side of the inclusion.

7) The presence of an inclusion changes the position of the maximum force on the dislocation. The maximum force on the dislocation changes its position to $\theta = 60^{\circ}$ from $\theta = 70^{\circ}$ for static crack. With increasing value of the angle(ϕ) around the inclusion the force curves becomes more flat.

8) For a static crack, strain energy density is zero at crack tip($\theta = \pi$) and has a minimum in the direction $\theta = 0^{\circ}$. For a moving crack, the strain energy density plots have two fold symmetry around the crack. The crack will propagate along $\theta = 0^{\circ}$, since the crack has minimum strain energy density along $\theta = 0^{\circ}$ for crack speeds in the range $0 \leq$ å $\leq 0.6c_2$. At $0.8c_2$ strain energy density for crack is minimum along $\theta = 60^{\circ}$ and for speeds greater than $0.8c_2$ curves have minimum strain energy density along $\theta = 70^{\circ}$.

9) Total strain energy of crack increases with increasing crack speeds in the range $0 \leq$ å $\leq c_R$ and tends ti ınfinity at Rayleigh speed c_R. The instability of the crack increases with increasing crack speeds. At high speeds the crack bifurcates to minimize the energy of the system. At speeds greater than the c_R total strain energy of crack decreases

with increasing crack speeds.

10) The equivalent number of dislocations required to match the shear stress of a moving crack increases with increasing crack speeds, dislocation speeds and shear stress. The equivalent number of dislocation decreases with increasing radial distance from the crack tip. The number of dislocations required to match the shear stress is of the order 10^4 and has a non-linear variation with the radial distance from the crack tip.

11) The build up of dislocations at the crack tip results either in blunting of the crack tip when the crack surface acts as a barrier or leads to formation of a new crack in a direction perpendicular to the slip plane in the presence of an inclusion between the crack tip and the dislocation source or nucleation of a void at the inclusion and matrix interface depending upon the strength of the inclusion.

REFERENCES

1. Kobayashi, S. and Ohr, S.M., Phil. Mag. A42, 1980, P.763.
2. Rice, J.R. and Thomson, R., Phil. Mag. A29, 1973, P.73.
3. Atkinson, C., Int. J. Fracture Mech. 2, 1966, P.567.
4. Bilby, B.A., Cottrell, A.H. and Swinden, K.H., Proc. Roy. Soc. (London) A272, 1963, P.304.
5. Riedel, H., J. Mech. Phys. Solids 24, 1976, P.277.
6. Barnett, D.M., and Asaro, R. J.,J. Mech. Phys. Solids 20, 1972, P.353.
7. Louat, N. P., Proc. First Int. Conf. On Fracture (Sendai, Japan, 1965) pp.117 .
8. Hart, E., Int. J. Solid Struct. 16, 1980, P.807.
9. Ashby, M. and Embury, J., Scripta Metall. 19, 1985, P.557.
10. Lin, I. and Thomson, R., J. Mater. Res. 1, 1986, P.73.
11. Paskin, A., Sieradzki, K., Som, D. and Dienes, D.,Acta Metall. 31, 1983, P.1253.
12. Pugh, N., in Atomistics of fracture (edited by R. Latanision and J. Pickens, Plenum Press, N.Y. 1983) pp.997
13. Knott, J., J.Fundamental oF Fracture Mechanics, Butterworths, London (1973).
14. Idem , Scripta Met. 15, 1981, P.343.
15. Vitek, V., J. Mech. Phys. Solids 24, 1976, P.263.
16. Chang, S.J. and Ohr, S.M., "Dislocation Modelling of Physical System". (ed. by M.F. Ashby, et al., Prergamon, 1981) p.23
17. Chang, S.J. and Ohr, S.M., Int. J. Fracture 23, R3(1983).
18. Burns, S.J.and Majumdar, B.S., Int. J. Fracture 21, 1983, P.229.
19. Ohr, S.M. and Narayan, J., Phil. Mag. A41, 1980, P.81.

20. Majumdar, B.S. and Burns, S.J.,Scripta Met. 14, 1980, P.653

21. Thomson, R., Solid State Phys. 39, 1986, P.1

22. Lin, I.H. and Thomson, R., Acta metall. 34, 1986, P.187

23. Binns, D.B., in science of ceramics (ed. by G.H. stewart, Academic Press, N.Y. 1962, P.315

24. Green, D.J., Nicholson, P.S and Embury, J.D., J. Mater. Sci. 14, 1979, P.1657

25. Laugue, F.F., Phil. Mag. 22,1970, p.983

26. Liu, H.W., Trans. ASME, J.of Basic Engineering 92, 1970, P.633

27. Motto, N.F. and Nabarro, F.R.N., Proc. Phys. Soc.(london) 52, 1940, P.86

28. Weertman, J., Phil. Mag. A43, 1981, P.1103

29. Kelly, A., Tyson, W.R. and Cottrell, A.H., Phil. Mag. 15, 1967, P.567

30. Lardner, R.W., Mathematical Theory of Dislocations and Fracture, University of Toronto Press, Toronto(1974) .

31. Majumdar, B.S. and Burns, S.J., Acta Metall. 29, 1981, P.579

32. Ohr, S.M., J. Phys. Chem. Solids 48, 1987, P.1007

33. Zhang, T.Y. and Li, J.C.M., Mater. Sci. Engg. A142, 1991, P.35

34. Chia, K.Y. and Burns, S.J., Scripta Metall. 18, 1984, P.467

35. Asaro, R.J., J. Phys. F:5, 1975, P.2249

36. Warren, W.E., Proc. Sixth South Eastern Conf. On Theoretical and Applied Mechanics (Univ. of South Florida U.S.A., 1972) pp.889 .

37. Eshelby, J.D., Proc. Roy. Soc.(London) A241, 1957, P.376

38. Achenbach, J.D., Wave Propagation in Elastic Solid,

Amsterdam(1973), North-Holland .

39. Hellan, Käre, "Introduction to Fracture Mechanics", McGraw-Hill Book Company, N.Y. ,1984 .

40. Freund, L.B., "Dynamic Fracture Mechanics ", Cambridge University Press, Cambridge , 1990 .

41. Irwin, G.R., Fracture Mechanics, in Structural Mechanics , eds. J.N. Goodier and N.J. Hoff. Elmsford, N.Y., Pergamon, pp.557

42. Faber, K.J. and Evans, A.G., Acta Metall. 31, 1983, P.4

43. Eshelby, J.D., J. Applied Physics 25, 1954, P.255

44. Cottrell, A.H., "Dislocation and Plastic Flow in Crystals", Clarendon Press , Oxford, 1953.

45. Dieter, G.E.,"Mechanical Metallurgy", McGraw-Hill Book Company ,2nd edition, 1987 .

46. Bilby, A.H., Proc. Phys. Soc.(London) A63, 1950, P.191

47. Kayano, H., Trans, Japan Inst. Metals 9, 1968, P.156

48. Broek, D.,"Elementary Engineering Fracture Mechanics", 3rd edition, Hague, Martinus Nijhaff(1982).

49. Parton, V.z. and Morozov, E.M.," Elastic-Plastic Fracture Mechanics", Mir Publication, Mascow(1978).

50. Kochs, U.F., Argon, A.S. and Ashby, M.F.," Thermodynamics and Kinetics of Slip", Pergaueon Press(1975).

51. Hirth, J.P. and Lothe, J., "Theory of dislocation", McGraw-Hill, New york (1968).

52. Sih, G.C., Int. J. Fracture 10, 3(1974), p.305.

53. Weertman, J. and Weertman, J.R., in Dislocations in Solid, F.R.N. Nabarro, North-Holland (1980), p.3.

54. [illegible] P.T., Williams, J.A. and Hurrison, R.P., Scripta

Metall. 5, (1971), pp.543.

55. Shetty, M.N., in Metallurgical Applications of Shock-Wave and High-Strain-Rate Phenomena, Eds. L.E. Murr, et.al., Marcel Dekker, Inc., New York, 1986, pp.509.

56. Sinha, V.K., Shetty, M.N., and Singh, K.P., Trans. Faraday Soc., Vol.66, No.572, 8(1970), pp.1981.

57. Li, J.C.M., in Dislocation in Solid, edited by H. Suzuki et.al., University of Tokyo Press, 1985, PP.617.

APPENDICES - A

For small displacement a(t) <<< x and from Fig.(2.1)

$$\tan\theta = \frac{y}{x} \qquad x = r\cos\theta,\ y = r\sin\theta \tag{A.1}$$

$$r_i = \left(\xi^2 + \zeta_i^2\right)^{1/2} \tag{A.2}$$

Using eqn(2.1.3) and (A.1), eqn(A.2) becomes

$$r_i^2 = \left[r\cos\theta - a(t)\right]^2 + \delta_i^2\, r^2 \sin^2\theta$$

$$= r^2\cos^2\theta + a^2(t) - 2\, r\cos\theta\, a(t) + \delta_i^2\, r^2 \sin^2\theta \tag{A.3}$$

Neglecting the term $a^2(t)$ and $2\, r\cos\theta\, a(t)$,(A.3) becomes

$$r_i^2 = r^2\left[1 - \sin^2\theta + \delta_i^2 \sin^2\theta\right]$$

or, $$r_i = r\left[1 - (1 - \delta_i^2)\sin^2\theta\right]^{1/2} \tag{A.4}$$

Now, $$\theta_i = \tan^{-1}\left(\frac{\zeta_i}{\xi}\right) \tag{A.5}$$

Using eqn(2.1.3) , eqn (A.5) becomes

$$\tan\theta_i = \frac{\delta_i\, y}{x - a(t)}$$

$x >>> a(t)$,

$$\tan\theta_i = \delta_i\ \frac{y}{x}$$

or, $$\tan\theta_i = \delta_i\ \tan\theta \tag{A.6}$$

APPENDIX B

L'HOSPITAL's THEOREM: Let $\phi(x)$ and $\psi(x)$ be the functions which are expansible by Taylor's Theorem in the neighborhood of $x = a$. Also, $\phi(a) = 0$, and $\psi(a) = 0$. Then

$$\text{Lim}_{x \to a} \frac{\phi(x)}{\psi(x)} = \text{Lim}_{x \to a} \frac{\phi'(x)}{\psi'(x)}$$

In eqns(2.1.7) when velocity of crack tip $\dot{a}$ tend to zero all the components of stress become the form of $\frac{0}{0}$. Hence this is an indeterminate form, so limit is obtained by using L'Hospital's Theorem. Function D is common in all equations and this become zero, when $\dot{a} \to 0$. Differentiate eqn(2.1.8) w.r.t $\dot{a}$ and i becomes:

$$\frac{\partial D}{\partial \dot{a}} = 4\delta_1 \frac{\partial \delta_2}{\partial \dot{a}} + 4\delta_2 \frac{\partial \delta_1}{\partial \dot{a}} - 4\delta_2 \left(1 + \delta_2^2\right) \frac{\partial \delta_2}{\partial \dot{a}} \qquad \text{(B.1)}$$

Taking the limit of eqns(2.1.3) $\dot{a} \to 0$, we get

$$\text{Lim}_{\dot{a} \to 0} \delta_1 = \text{Lim}_{\dot{a} \to 0} \delta_2 = 1 \qquad \text{(B.2)}$$

Differentiate the eqns(2.1.3) w.r.t $\dot{a}$, we get

$$\frac{\partial \delta_1}{\partial \dot{a}} = - \frac{\dot{a}}{c_1^2 \delta_1}, \quad \frac{\partial \delta_2}{\partial \dot{a}} = - \frac{\dot{a}}{c_2^2 \delta_2} \qquad \text{(B.3)}$$

Substitute the values from equations (B.3) in eqn(B.1) and taking the limit as $\dot{a}$ tends to zero and simplified it becomes

$$\text{Lim}_{\dot{a} \to 0} \left[\frac{1}{\dot{a}} \frac{\partial D}{\partial \dot{a}}\right] = - 4 \left[\frac{1}{c_1^2} - \frac{1}{c_2^2}\right] \qquad \text{(B.4)}$$

Now from eqn(2.1.7) differentiate f_{11} components of stress w.r.t. $\dot{a}$

$$\frac{\partial f_{11}}{\partial \dot{a}} = \left[2\delta_2 \frac{\partial \delta_2}{\partial \dot{a}} \left(1 + 2\delta_1^2 - \delta_2^2\right) + \left(1 + \delta_2^2\right)\left(4\delta_1 \frac{\partial \delta_1}{\partial \dot{a}} - 2\delta_2\right.\right.$$

$$\frac{\partial \delta_2}{\partial \mathring{a}}\Big)\Big] \frac{\cos(\theta_1/2)}{\sqrt{\gamma_1}} - \left(1 + \delta_2^2\right)\left(1 + 2\delta_1^2 - \delta_2^2\right) \frac{\sin(\theta_1/2)}{2\sqrt{\gamma_1}}$$

$$\frac{\partial \theta_1}{\partial \mathring{a}} - \left(1 + \delta_2^2\right)\left(1 + 2\delta_1^2 - \delta_2^2\right) \frac{\cos(\theta_1/2)}{2\,\gamma_1^{3/2}} \frac{\partial \gamma_1}{\partial \mathring{a}} - 4\Big(\delta_2$$

$$\frac{\partial \delta_1}{\partial \mathring{a}} + \delta_1 \frac{\partial \delta_2}{\partial \mathring{a}}\Big) \frac{\cos(\theta_2/2)}{\sqrt{\gamma_2}} + 2\delta_1\,\delta_2 \frac{\sin(\theta_2/2)}{2\sqrt{\gamma_2}} \frac{\partial \theta_2}{\partial \mathring{a}} +$$

$$2\delta_1\delta_2 \frac{\cos(\theta_2/2)}{2\,\gamma_2^{3/2}} \frac{\partial \gamma_2}{\partial \mathring{a}} \qquad \text{(B.5)}$$

Differentiate eqn(2.1.5) w.r.t. å, we get

$$\frac{\partial \theta_i}{\partial \mathring{a}} = \frac{\tan\theta}{1 + \delta_i^2 \tan^2\theta} \frac{\partial \delta_i}{\partial \mathring{a}} \qquad \text{(B.6)}$$

Taking the limit of eqn(2.1.5), we get

$$\theta_i = \theta \text{ as } \mathring{a} \to 0 \qquad \text{(B.7)}$$

Differentiate eqn(2.1.9) w.r.t. å and on arranging the terms we get

$$\gamma_i^{-3/2} \frac{\partial \theta_i}{\partial \mathring{a}} = -\mathring{a}\left[\frac{\sin\theta}{c_i}\right]^2 \left[1 - \left(\frac{\mathring{a}\sin\theta}{c_i}\right)^2\right]^{-5/4} \qquad \text{(B.8)}$$

Taking the limit of eqn(2.1.9), we get

$$\gamma_i = 1 \text{ as } \mathring{a} \to 0 \qquad \text{(B.9)}$$

Put the value from eqns(B.3), (B.6) and (B.8) in eqn(B.5) and taking the limit, we get

$$\text{Lim}_{\mathring{a} \to 0}\left[\frac{1}{\mathring{a}} \frac{\partial f_{11}}{\partial \mathring{a}}\right] = -4\left[\frac{1}{c_1^2} - \frac{1}{c_2^2}\right]\left[1 - \sin\theta/2\,\sin 3\theta/2\right]\cos\theta/2 \qquad \text{(B.10)}$$

Divide eqn(B.10) and Eqn(B.4), we get $f_{11}(\theta)$ for static crack:

$$f_{11}(\theta) = \left[1 - \sin\theta/2\,\sin 3\theta/2\right]\cos\theta/2 \qquad \text{(B.11)}$$

Now from eqn(2.1.7) differentiate fzz component of stress w.r.t.å

$$\frac{\partial f_{zz}}{\partial \mathring{a}} = -4\delta_2 \frac{\partial \delta_2}{\partial \mathring{a}} \left(1 + \delta_2^2\right) \frac{\cos(\theta_1/2)}{\sqrt{\gamma_1}} + \left(1 + \delta_2^2\right)^2 \frac{\sin(\theta_1/2)}{2\sqrt{\gamma_1}} \frac{\partial \theta_1}{\partial \mathring{a}} + \left(1 + \delta_2^2\right)^2 \frac{\cos(\theta_1/2)}{2\gamma_1^{3/2}} \frac{\partial \gamma_1}{\partial \mathring{a}} + 4\left(\delta_2 \frac{\partial \delta_1}{\partial \mathring{a}} + \delta_1 \frac{\partial \delta_2}{\partial \mathring{a}}\right) \frac{\cos(\theta_2/2)}{\sqrt{\gamma_2}} - 2\delta_1 \delta_2 \frac{\sin(\theta_2/2)}{2\sqrt{\gamma_2}} \frac{\partial \theta_2}{\partial \mathring{a}} - 2\delta_1 \delta_2 \frac{\cos(\theta_2/2)}{2\gamma_2^{3/2}} \frac{\partial \gamma_2}{\partial \mathring{a}} \qquad (B.12)$$

Put the values from equations(B.3), (B.6) and (B.8) in eqn(B.12) and taking the limit, we get

$$\mathrm{Lim}_{\mathring{a} \to 0}\left[\frac{1}{\mathring{a}} \frac{\partial f_{zz}}{\partial \mathring{a}}\right] = -4\left[\frac{1}{c_1^2} - \frac{1}{c_2^2}\right]\left[1 + \sin\theta/2 \sin 3\theta/2\right]\cos\theta/2 \qquad (B.13)$$

Divide the eqn(B.13) and eqn(B.4), we get $f_{zz}(\theta)$ for static crack:

$$f_{zz}(\theta) = \left[1 + \sin\theta/2 \sin 3\theta/2\right] \cos\theta/2 \qquad (B.14)$$

Now from eqns(2.1.7) differentiate the f_{12} component of stress w.r.t $\mathring{a}$

$$\frac{\partial f_{12}}{\partial \mathring{a}} = \left[\frac{\cos(\theta_1/2)}{2\sqrt{\gamma_1}} \frac{\partial \theta_1}{\partial \mathring{a}} - \frac{\cos(\theta_2/2)}{2\sqrt{\gamma_2}} \frac{\partial \theta_2}{\partial \mathring{a}} - \frac{\sin(\theta_1/2)}{2\gamma_1^{3/2}} \frac{\partial \gamma_1}{\partial \mathring{a}} + \frac{\sin(\theta_2/2)}{2\gamma_2^{3/2}} \frac{\partial \gamma_2}{\partial \mathring{a}}\right]\left(1 + \delta_2^2\right) + \left[\frac{\sin(\theta_1/2)}{\sqrt{\gamma_1}} - \frac{\sin(\theta_2/2)}{\sqrt{\gamma_2}}\right] 2\delta_2 \frac{\partial \delta_2}{\partial \mathring{a}} \qquad (B.15)$$

Put the values from equations(B.6) and (B.8) in eqn(B.15) and taking the limit we get

$$\mathrm{Lim}_{\mathring{a} \to 0}\left[\frac{1}{\mathring{a}} \frac{\partial f_{12}}{\partial \mathring{a}}\right] = -4\left[\frac{1}{c_1^2} - \frac{1}{c_2^2}\right] \sin\theta/2 \cos 3\theta/2 \cos\theta/2 \qquad (B.16)$$

Divide the eqn(B.16) and (B.4), we get $f_{12}(\theta)$ component of stress for static crack:

$$f_{12}(\theta) = \sin(\theta/2)\cos(\theta/2)\cos(3\theta/2) \qquad (B.17)$$

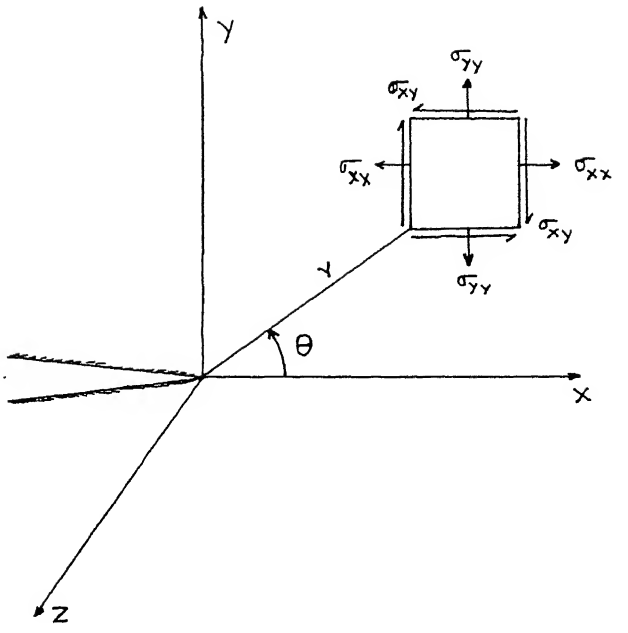

(a)

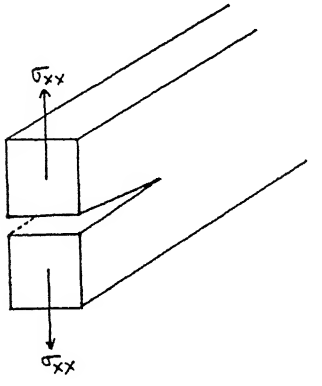

(b)

Fig(2.1) - (a) The state of stress for mode I crack.
(b) Mode I crack

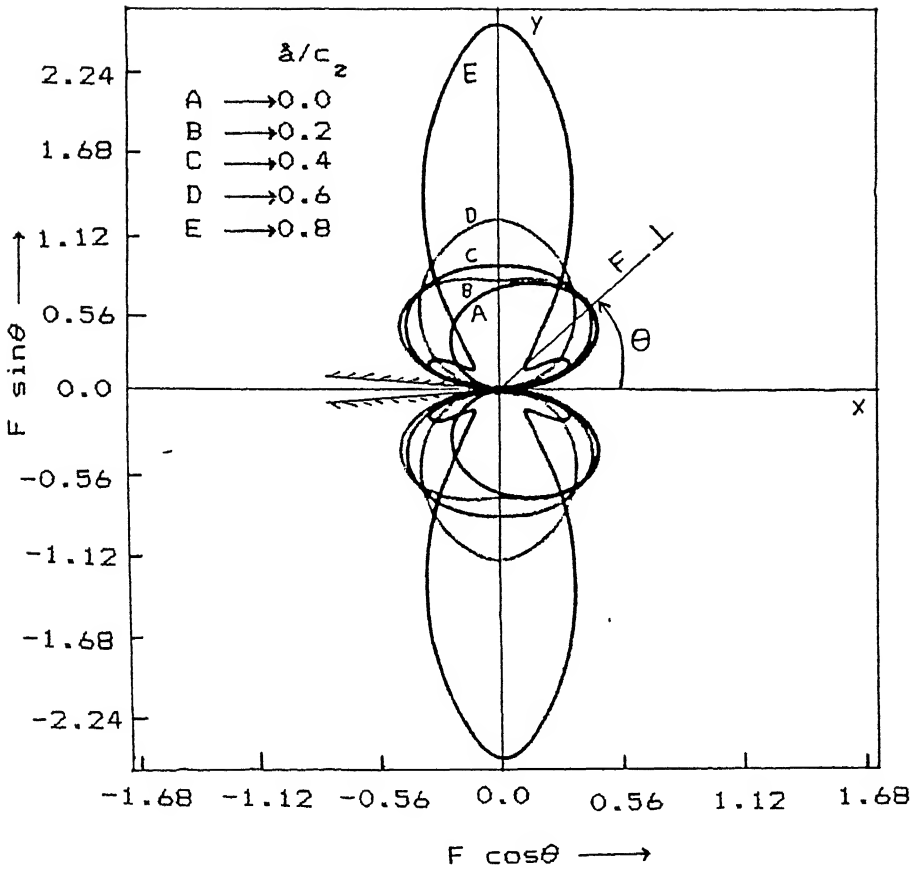

Fig.(2.2a) – The variation of force on a dislocation ($F = \sigma'_{12} b$) around a crack tip for a fixed radial distance in velocities range $0.0 \leq$ å $\leq 0.8c_z$.

σ'_{12} = Transformed shear stress on the glide plane of dislocation

b(Burger vector of dislocation) = 2.48Å

ν(Poisson ratio) = 0.333

G(Shear modulus of matrix) = 73 Gpa

K_I(Stress intensity factor) = 65 Mpa$\sqrt{m}$

r(Radial distance) = 10μm

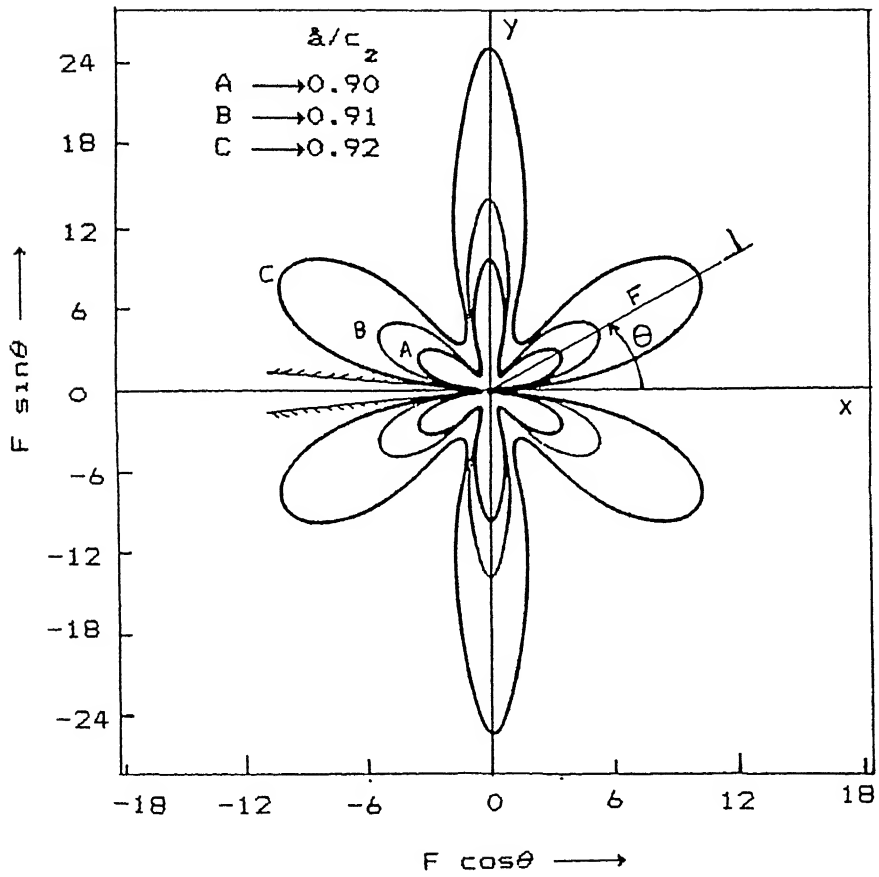

Fig.(2.2b) – The variation of force on a dislocation ($F = \sigma'_{12} b$) around a crack tip for a fixed radial distance in velocities range $0.90c_z \leq \dot{a} \leq 0.92c_z$.

σ'_{12} = Transformed shear stress on the glide plane of dislocation

b = 2.48Å, ν = 0.333, G = 73 Gpa, K_I = 65 Mpa$\sqrt{m}$,

r = 10μm

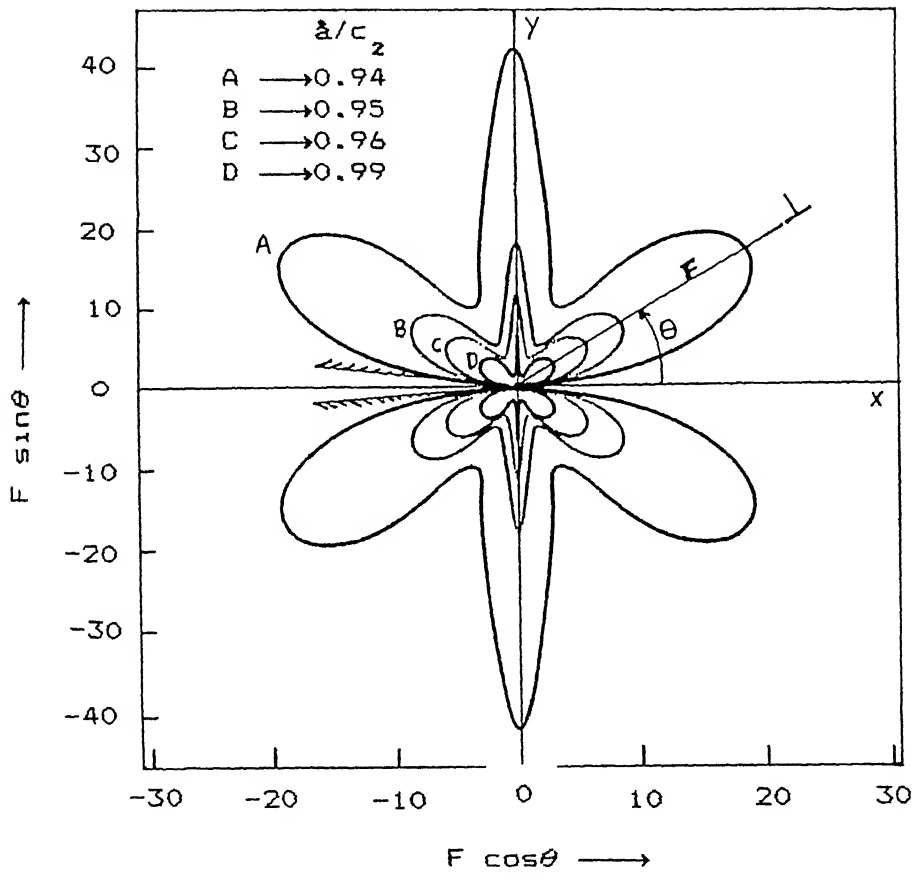

Fig.(2.2c) - The variation of force on a dislocation ($F = \sigma'_{12} b$) around a crack tip for a fixed radial distance in velocities range $0.94c_2 \leq \dot{a} \leq c_2$.

σ'_{12} = Transformed shear stress on the glide plane of dislocation

b = 2.48Å, ν = 0.333, G = 73 Gpa, K_I = 65 Mpa$\sqrt{m}$,

r = 10μm

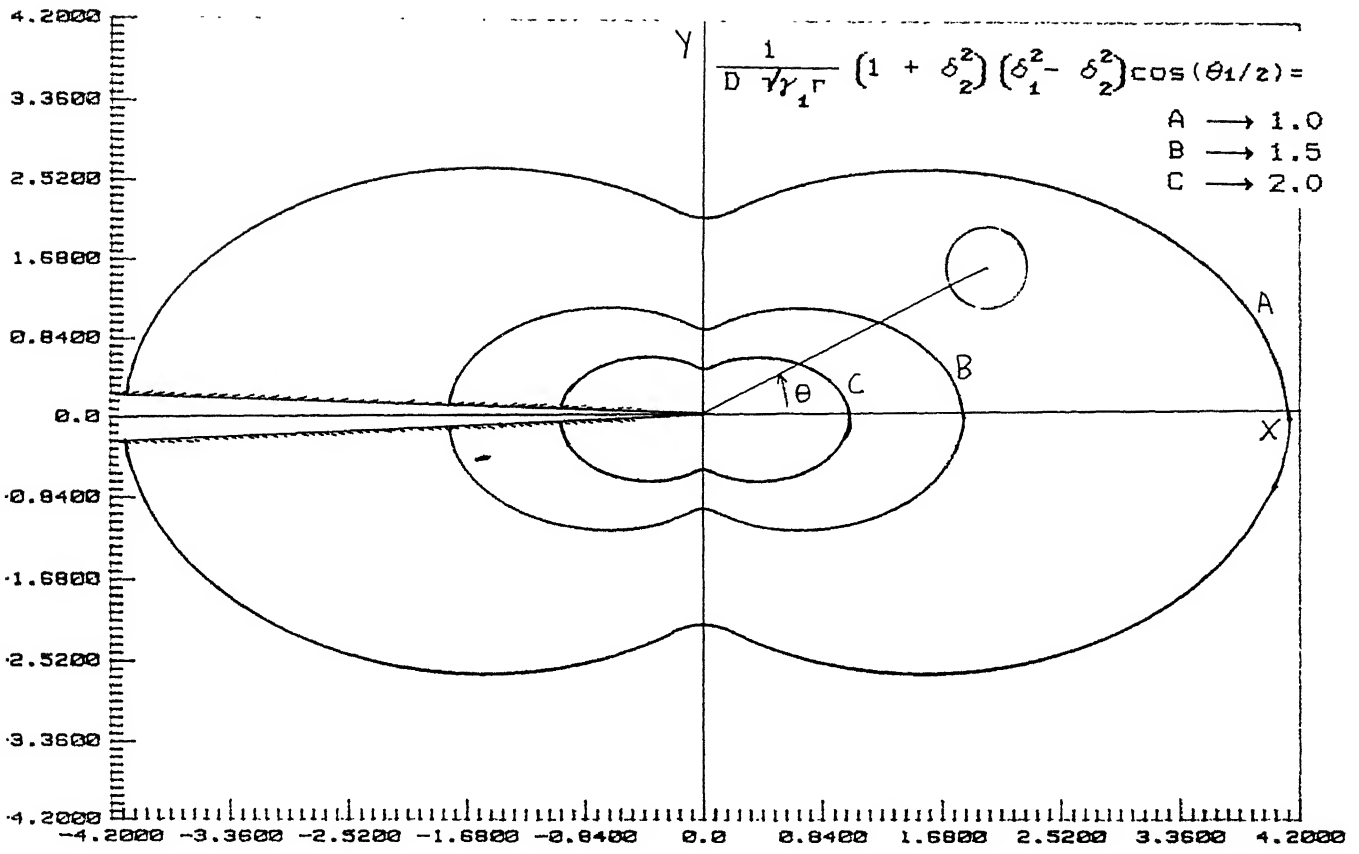

Fig.(2.3a) - Equipotential contours of constant value of $\frac{1}{D\sqrt{\gamma_1 r}}\left(1+\delta_2^2\right)\left(\delta_1^2-\delta_2^2\right)\cos(\theta_1/2)$ at crack tip velocity $\dot{a} = 0.2c_2$ for moving crack and inclusion interaction.

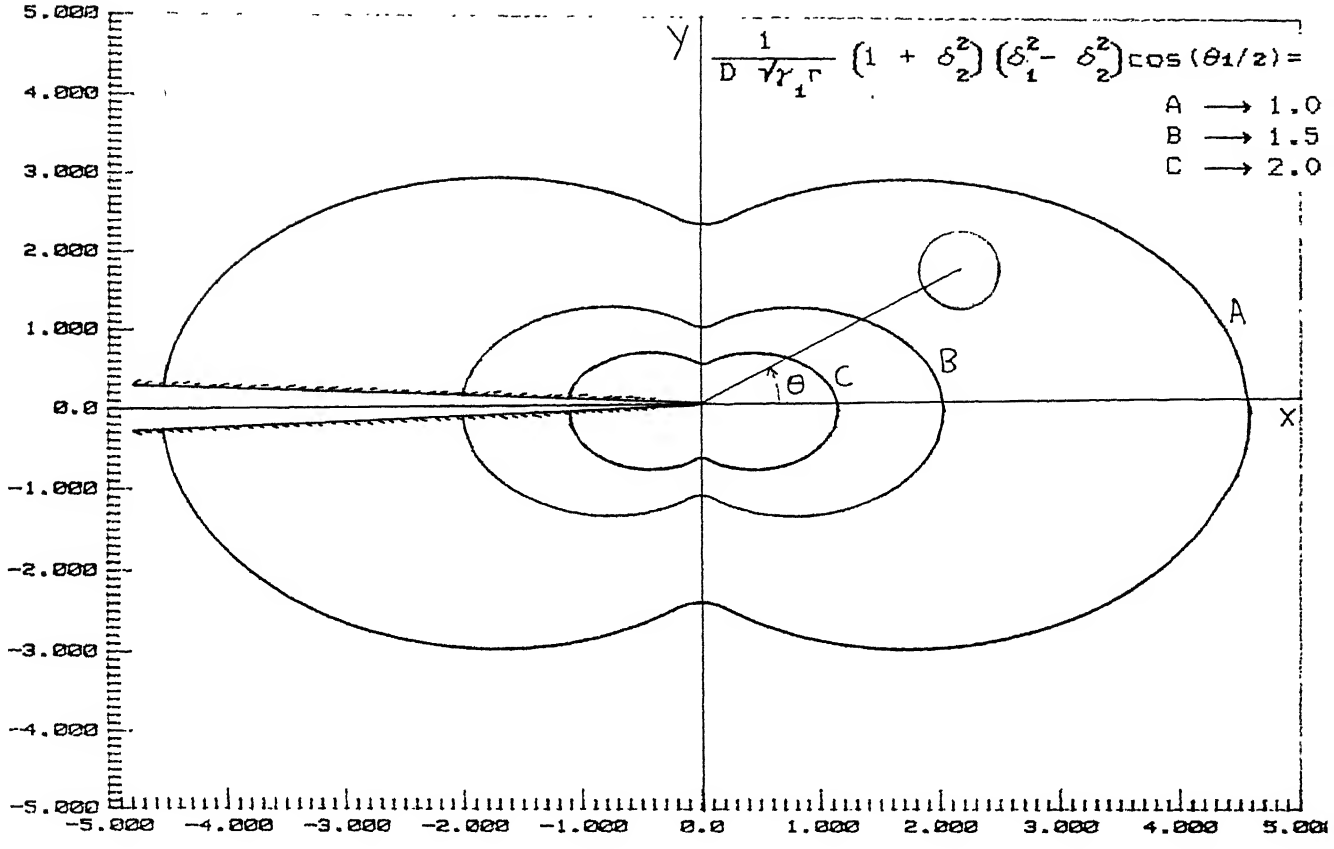

Fig.(2.3b) - Equipotential contours of constant value of $\frac{1}{D\sqrt{\gamma_1 r}}\left(1+\delta_2^2\right)\left(\delta_1^2-\delta_2^2\right)\cos(\theta_1/2)$ at crack tip velocity $\dot{a} = 0.4c_2$ for moving crack and inclusion interaction.

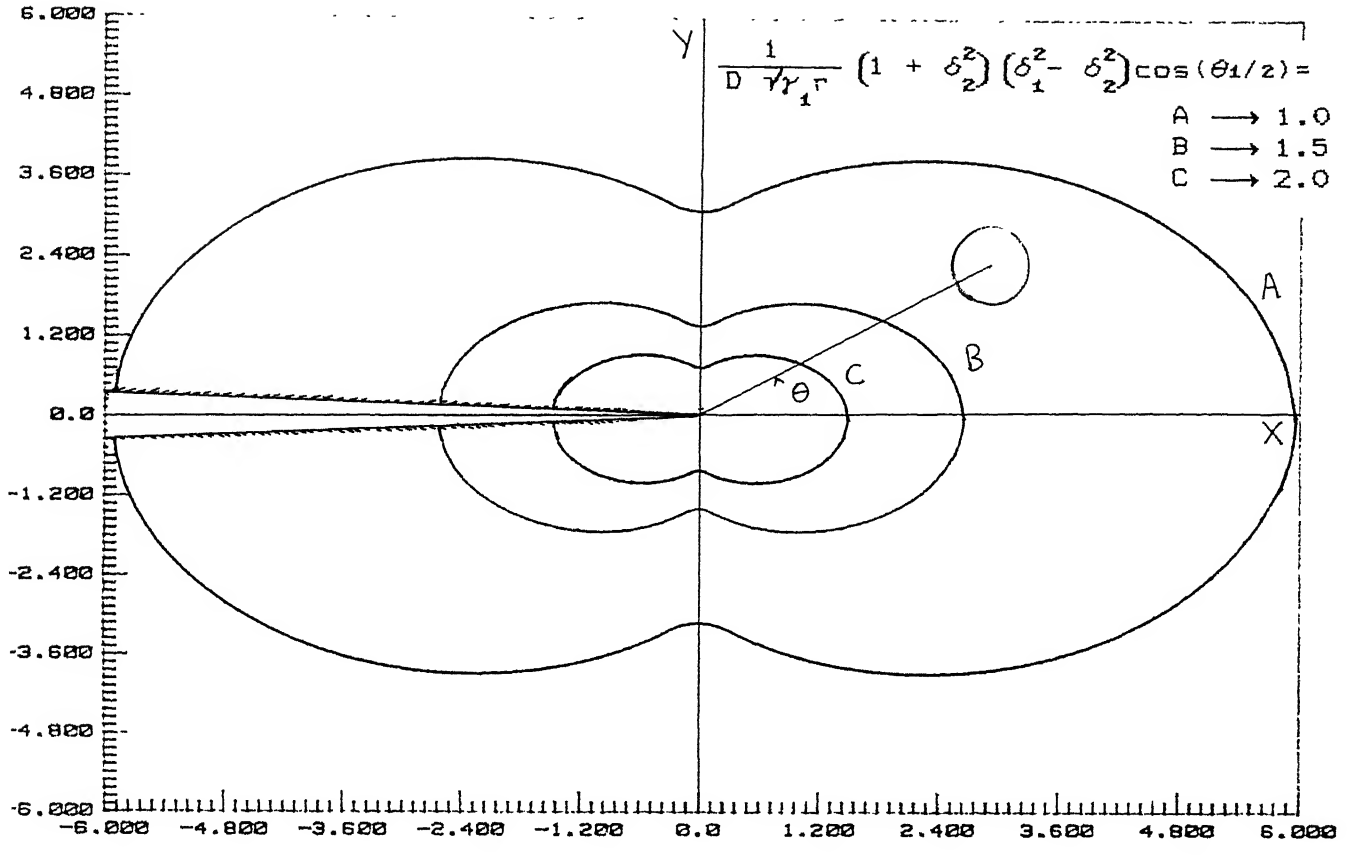

Fig.(2.3c) - Equipotential contours of constant value of $\frac{1}{D\sqrt{\gamma\gamma_1 r}}\left(1+\delta_2^2\right)\left(\delta_1^2-\delta_2^2\right)\cos(\theta_1/2)$ at crack tip velocity $\dot{a} = 0.6c_2$ for moving crack and inclusion interaction.

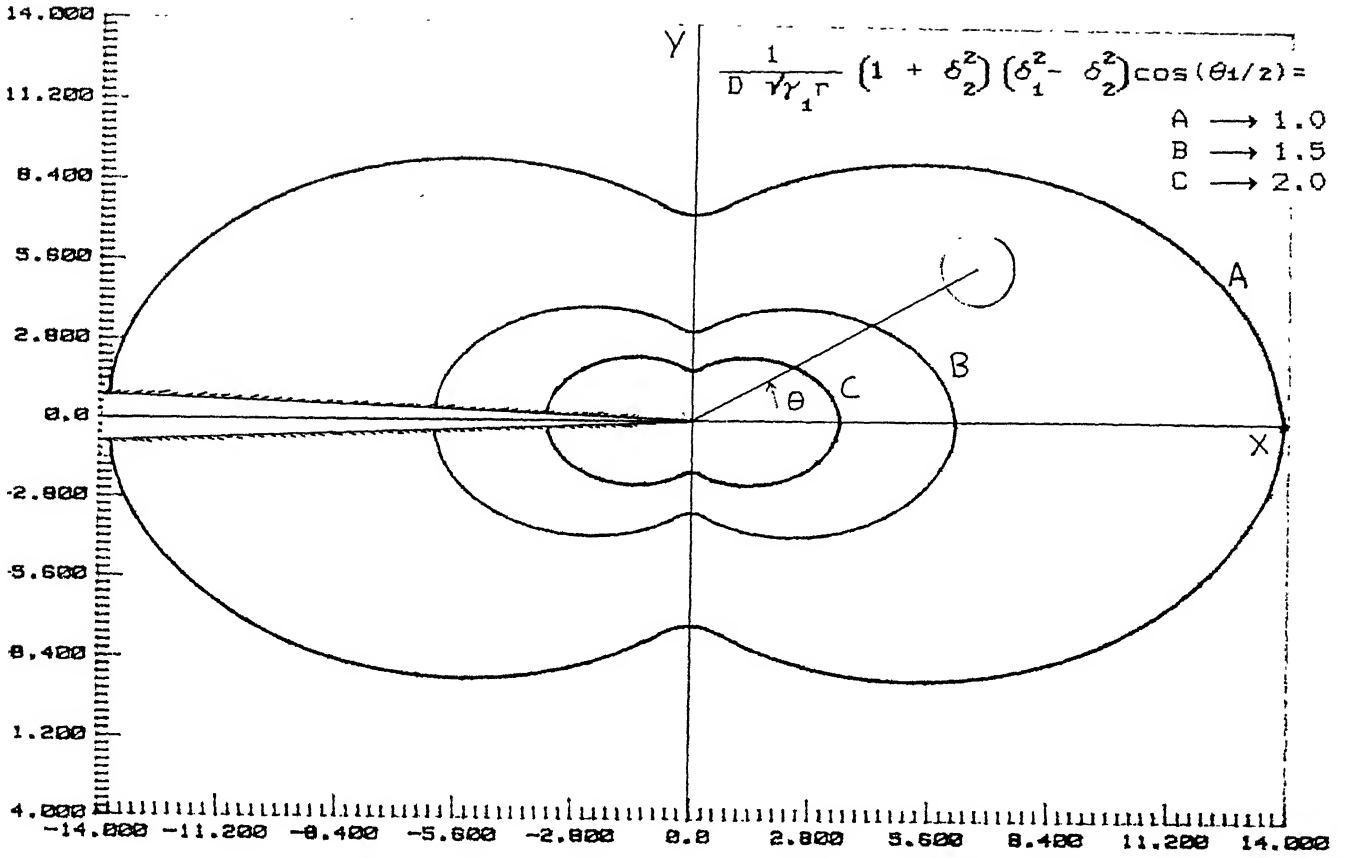

Fig.(2.3d) - Equipotential contours of constant value of $\frac{1}{D\sqrt{\gamma\gamma_1 r}}\left(1+\delta_2^2\right)\left(\delta_1^2-\delta_2^2\right)\cos(\theta_1/2)$ at crack tip velocity $\dot{a} = 0.8c_2$ for moving crack and inclusion interaction.

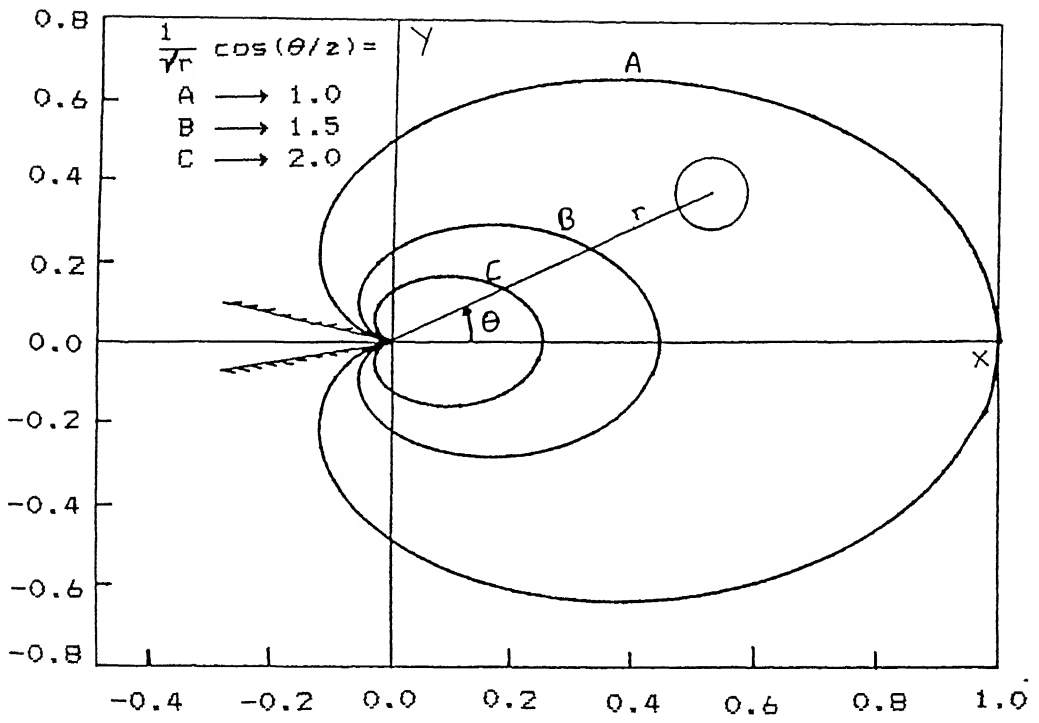

Fig.(2.4) - Equipotential contours of constant value of $\frac{1}{\sqrt{r}}\cos(\theta/2)$ for a static crack and inclusion interaction.

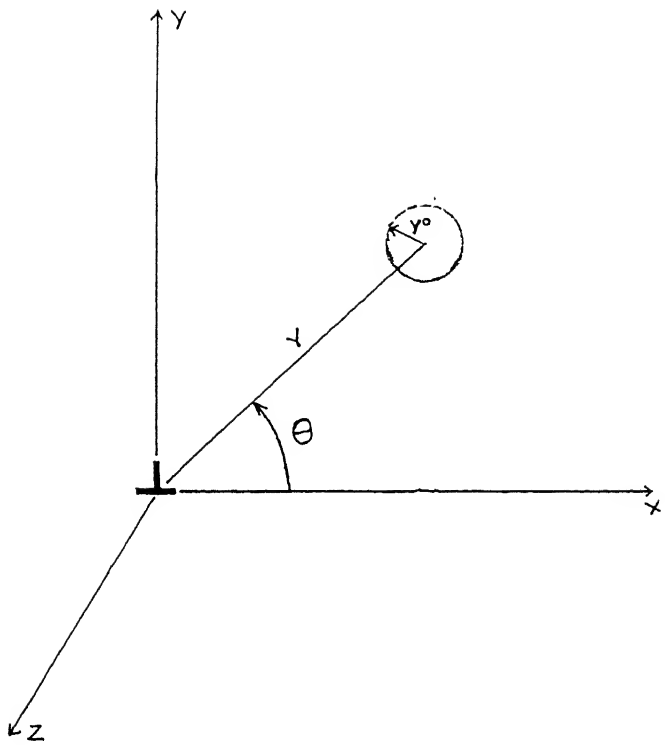

Fig (25)

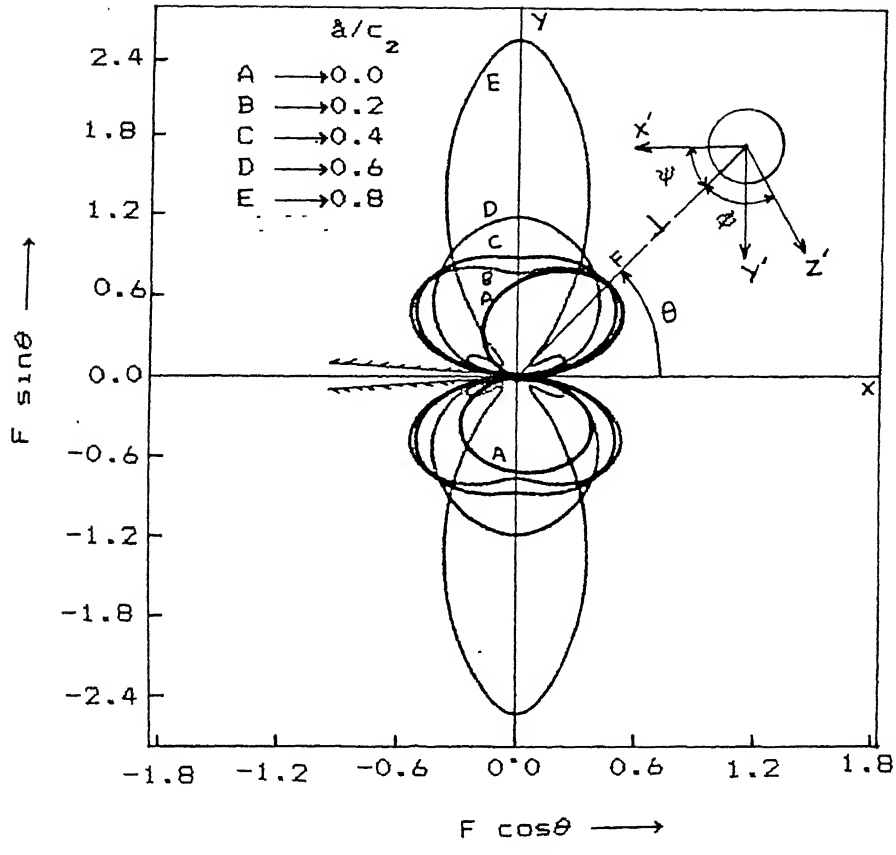

Fig.(2.6a) – The variation of force on a dislocation ($F = \sigma^{T}_{12} b$) around a crack tip for a fixed radial distance in velocities range $0.0 \leq å \leq 0.8c_z$.

$$\sigma^{T}_{12} = \sigma'_{12} + \sigma^{I}_{12}$$

σ^{T}_{12} = Total shear stress on the dislocation

σ'_{12} = Transformed shear stress on the glide plane of dislocation

σ^{I}_{12} = Transformed inclusion shear stress on glide plane of dislocation for $\phi = 30^{o}$ and $r°/r' = 0.8$

$b = 2.48Å$, $\nu = 0.333$, $G = 73$ Gpa, $K_I = 65$ Mpa$\sqrt{m}$,

$\mu = 156$ Gpa, $r = 10\mu m$, $r° = 4.2Å$.

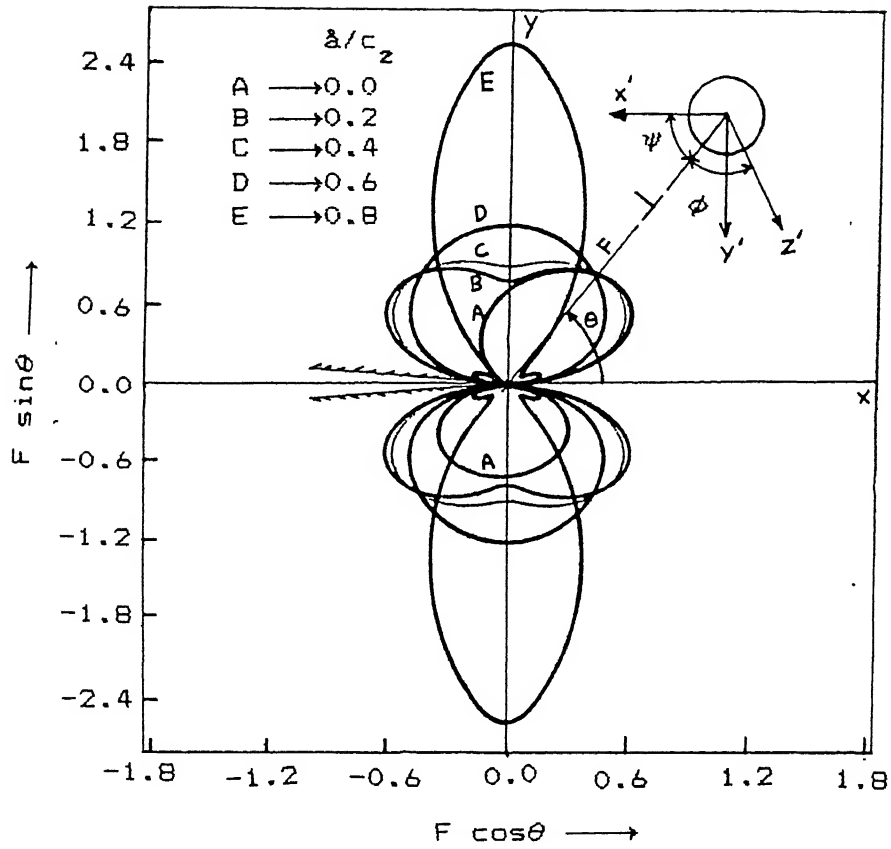

Fig.(2.6b) - The variation of force on a dislocation ($F = \sigma^{T}_{12} b$) around a crack tip for a fixed radial distance in velocities range $0.0 \leq \dot{a} \leq 0.8c_z$.

$$\sigma^{T}_{12} = \sigma'_{12} + \sigma^{I}_{12}$$

σ^{I}_{12} = Transformed inclusion shear stress on glide plane of dislocation for $\phi = 45^{o}$ and $r^{o}/r' = 0.8$

$b = 2.48\text{Å}$, $\nu = 0.333$, $G = 73$ Gpa, $K_I = 65$ Mpa$\sqrt{m}$,

$\mu = 156$ Gpa, $r = 10\mu m$, $r^{o} = 4.2\text{Å}$.

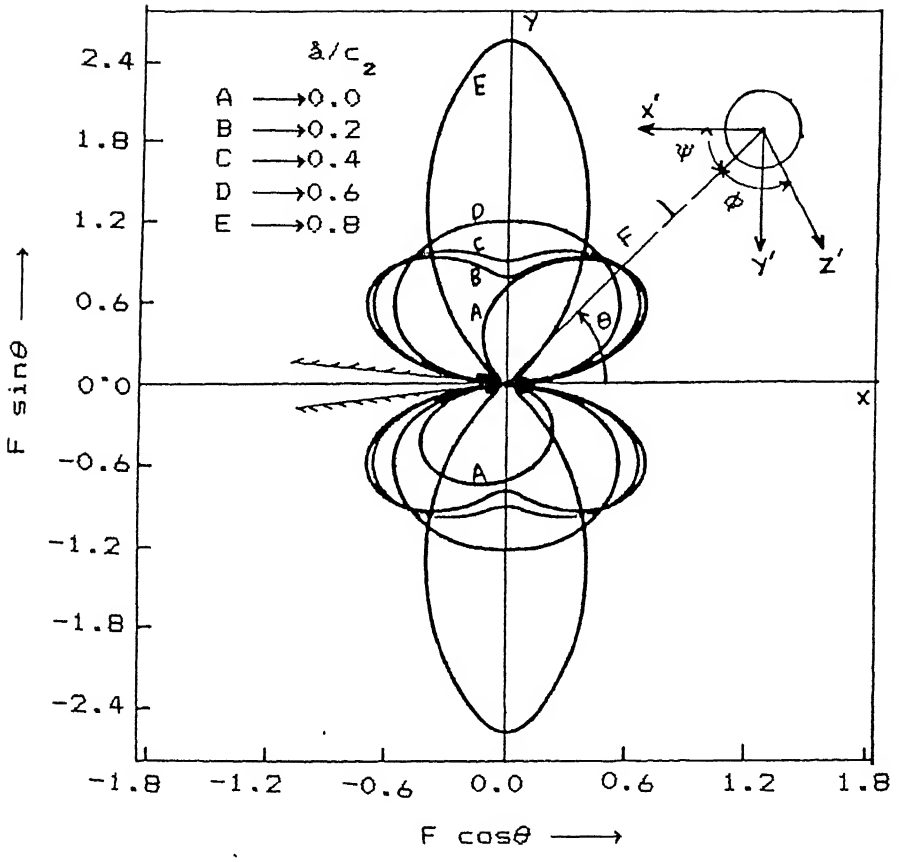

Fig.(2.6c) – The variation of force on a dislocation ($F = \sigma^{T}_{12} b$) around a crack tip for a fixed radial distance in velocities range $0.0 \leq \dot{a} \leq 0.8c_2$.

$$\sigma^{T}_{12} = \sigma'_{12} + \sigma^{I}_{12}$$

σ^{I}_{12} = Transformed inclusion shear stress on glide plane of dislocation for $\phi = 60^{\circ}$ and $r^{\circ}/r' = 0.8$

$b = 2.48\text{Å}$, $\nu = 0.333$, $G = 73$ Gpa, $K_I = 65$ Mpa$\sqrt{m}$,

$\mu = 156$ Gpa, $r = 10\mu m$, $r^{\circ} = 4.2\text{Å}$.

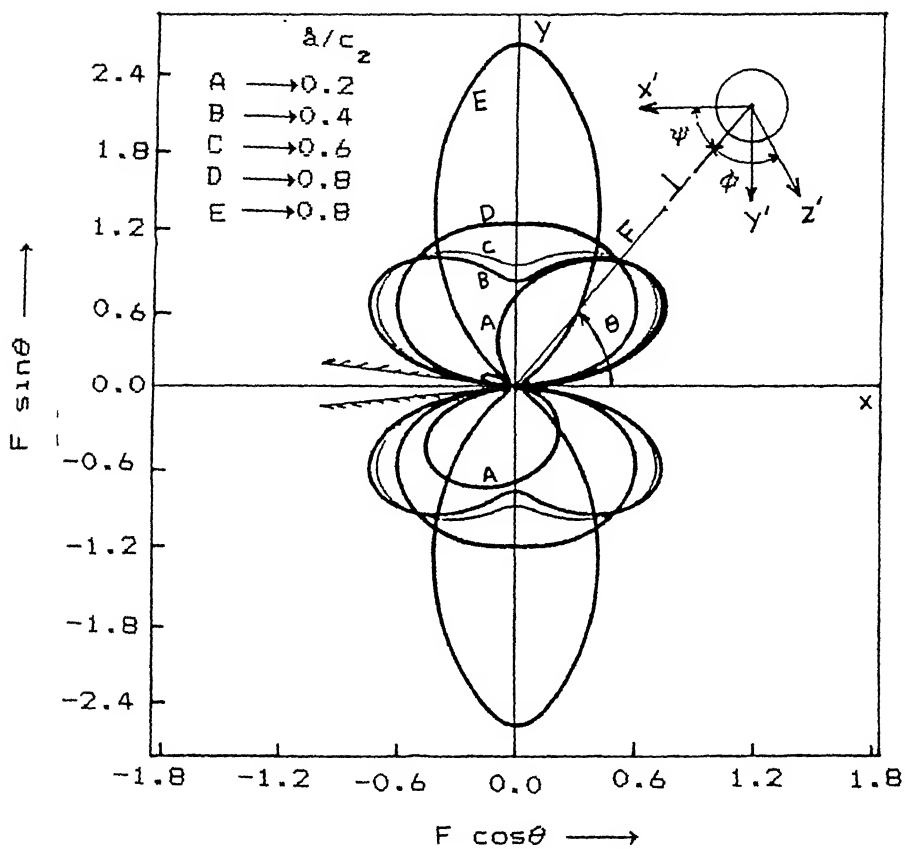

Fig.(2.6d) - The variation of force on a dislocation ($F = \sigma^{T}_{12} b$) around a crack tip for a fixed radial distance in velocities range $0.0 \leq \dot{a} \leq 0.8c_z$.

σ^{I}_{12} = Transformed inclusion shear stress on glide plane of dislocation for $\phi = 70^{o}$ and $r^{o}/r' = 0.8$

b = 2.48Å, ν = 0.333, G = 73 Gpa, K_I = 65 Mpa$\sqrt{m}$,

μ = 156 Gpa, r = 10μm, r^{o} = 4.2Å.

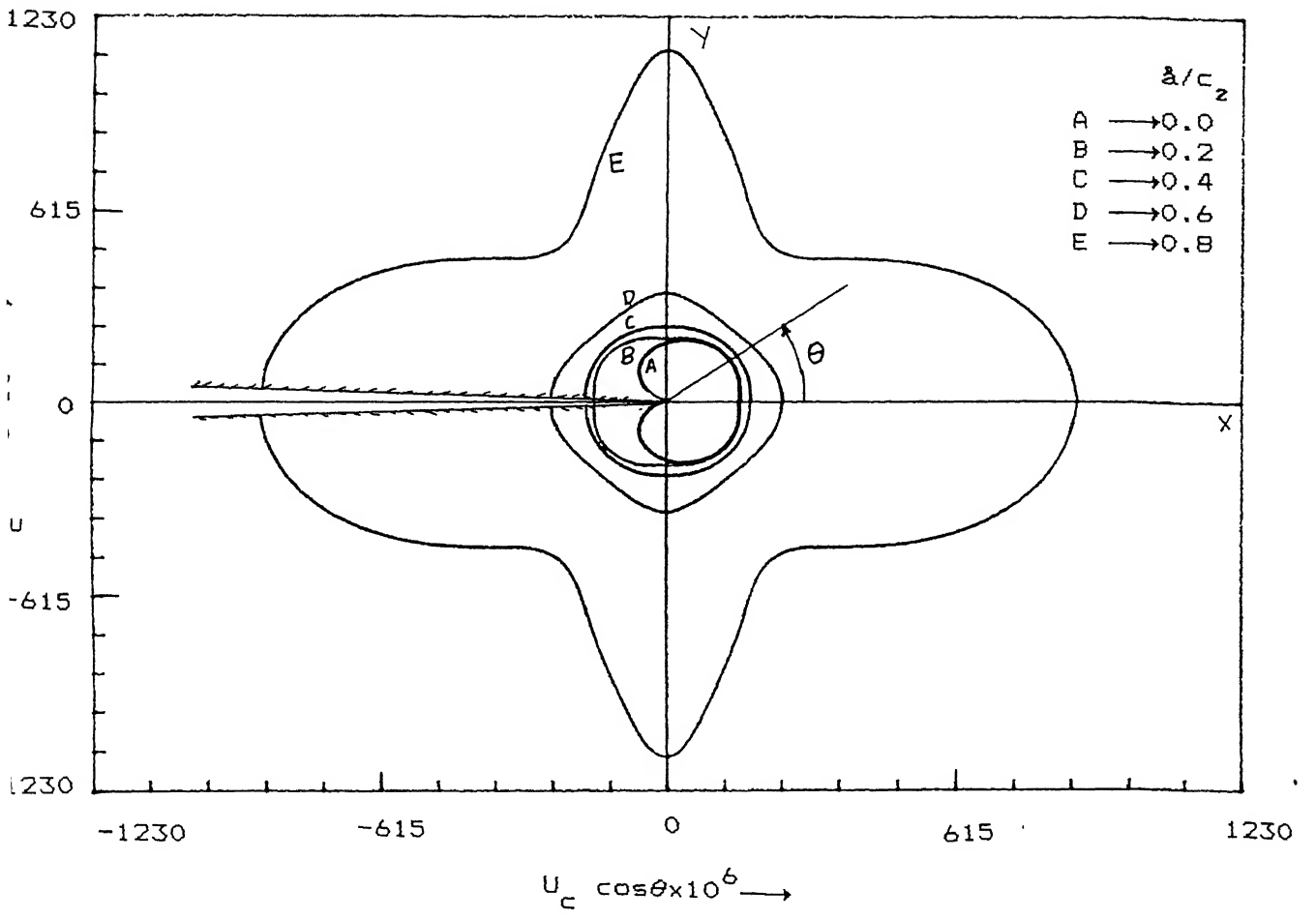

Fig.(2.7) - The distribution of the elastic strain energy density at the crack tip for values of θ varying between 0^{o} and 360^{o} and for normalized crack tip velocities 0.0, 0.2, 0.4, 0.6, 0.8.

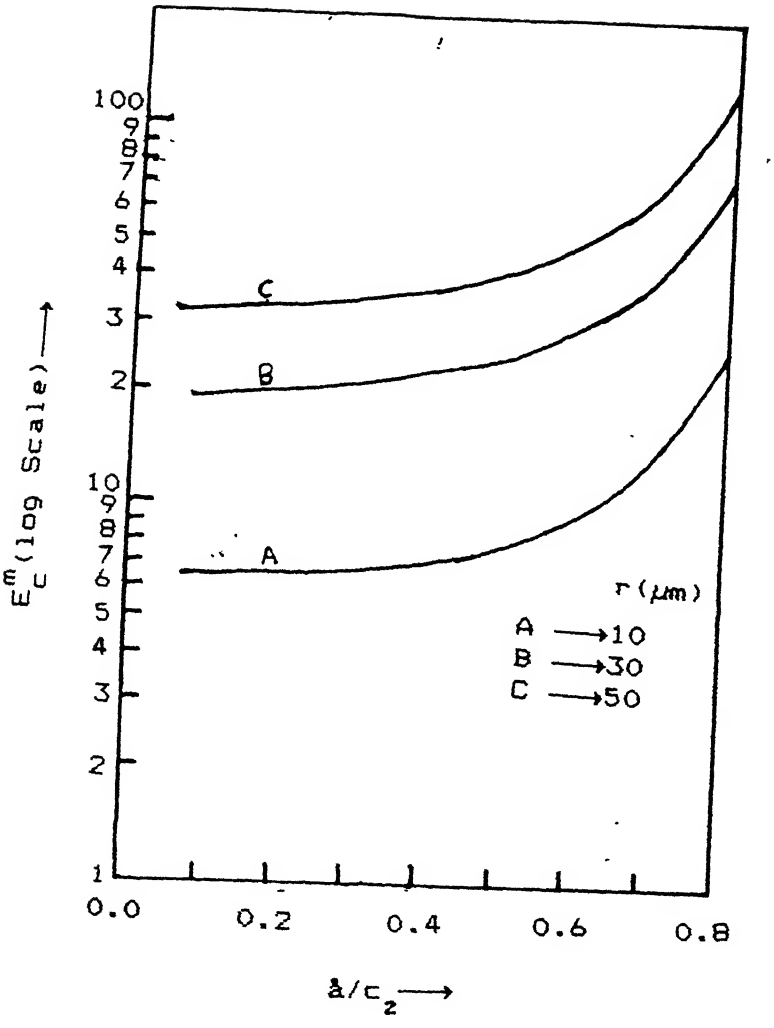

Fig.(2.8a) - The distribution of crack energy at 10μm radial distance from crack tip for normalized crack tip velocity varying between 0.0 and 0.8c_z.

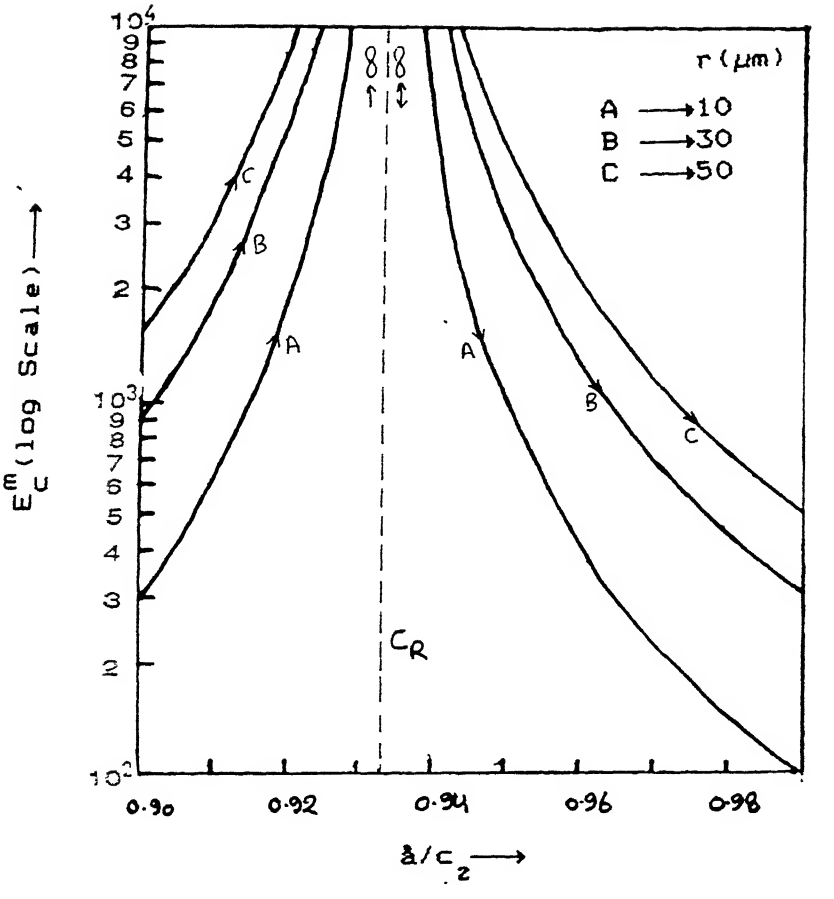

Fig.(2.8b) - The distribution of crack energy at 10μm radial distance from crack tip for normalized crack tip velocity varying between $0.90c_2$ and c_2.

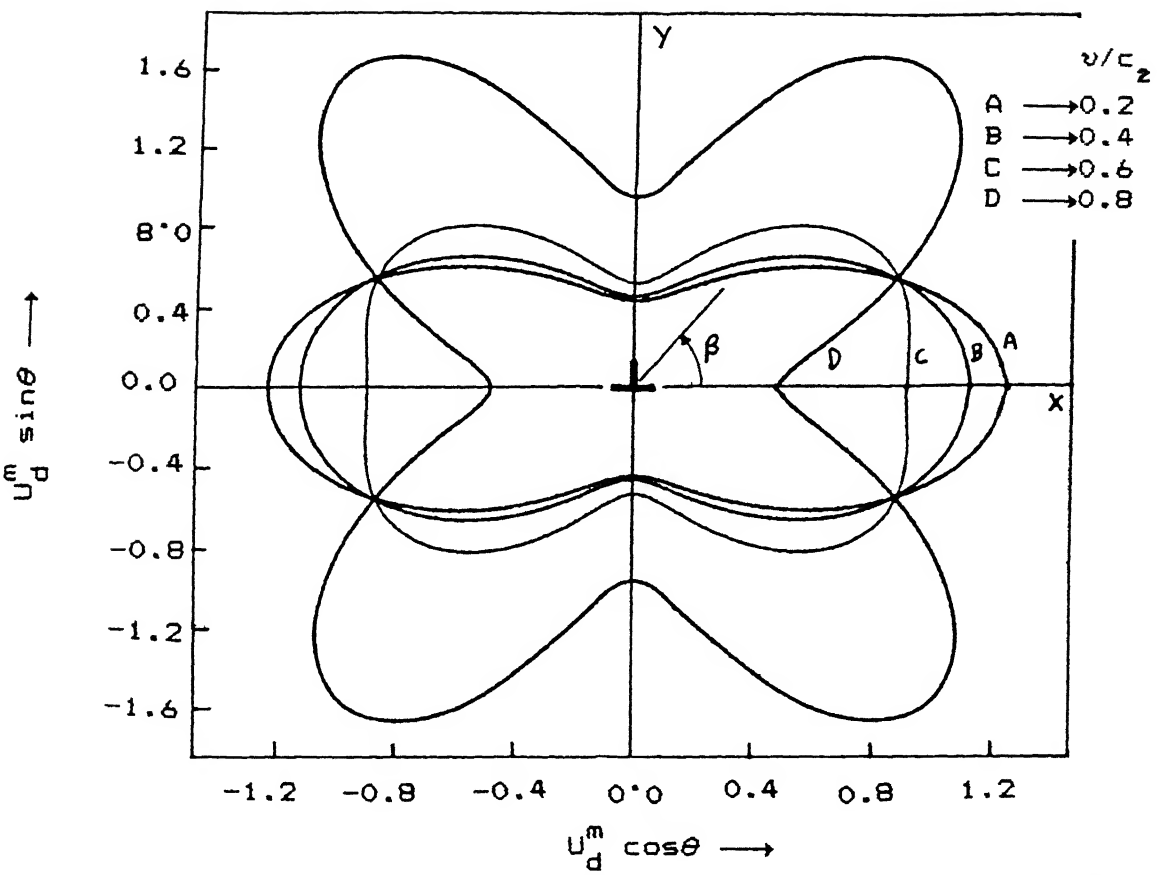

Fig.(2.9) - The distribution of the elastic strain energy density around the dislocation for value of θ varying between 0^o and 360^o and for normalized dislocation velocities 0.2, 0.4, 0.6, 0.8.

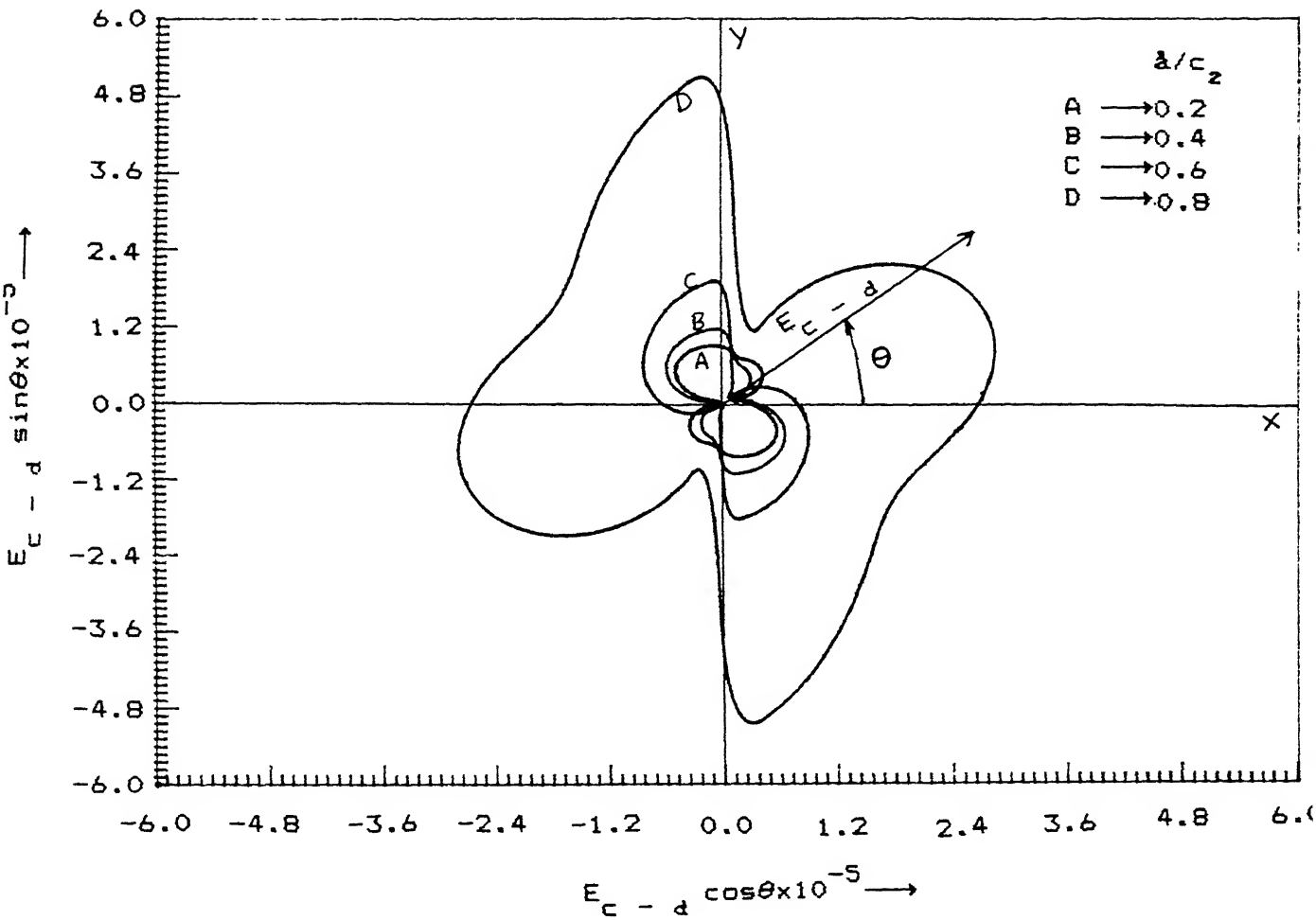

Fig.(2.10) – The variation of interaction energy E_{c-d} between crack and dislocation with θ for a fixed radial distance and for normalized crack tip velocities 0.2, 0.4, 0.6, 0.8.

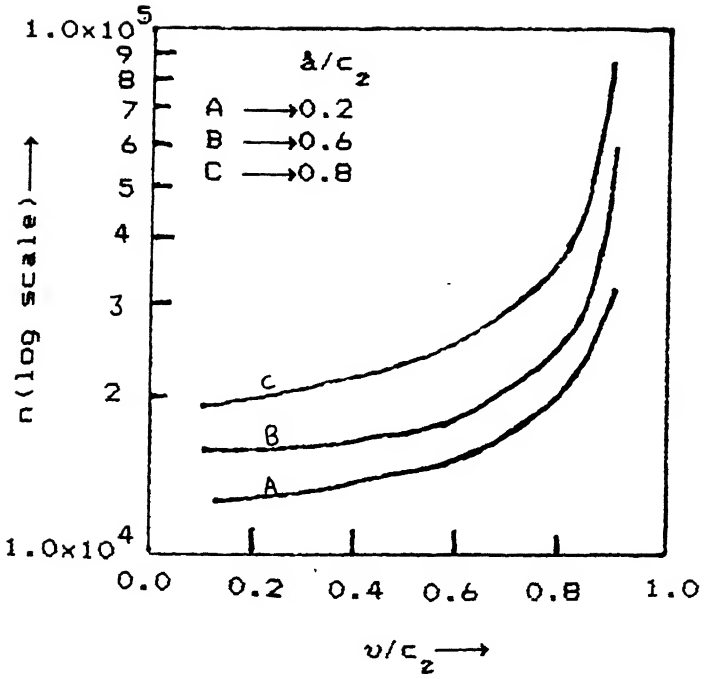

Fig.(2.11) - The variation of number of dislocations(n) with normalized dislocation velocity(υ/c_2) for a fixed radial distance r = 10μm and at normalized crack tip velocities 0.2, 0.6, 0.8.

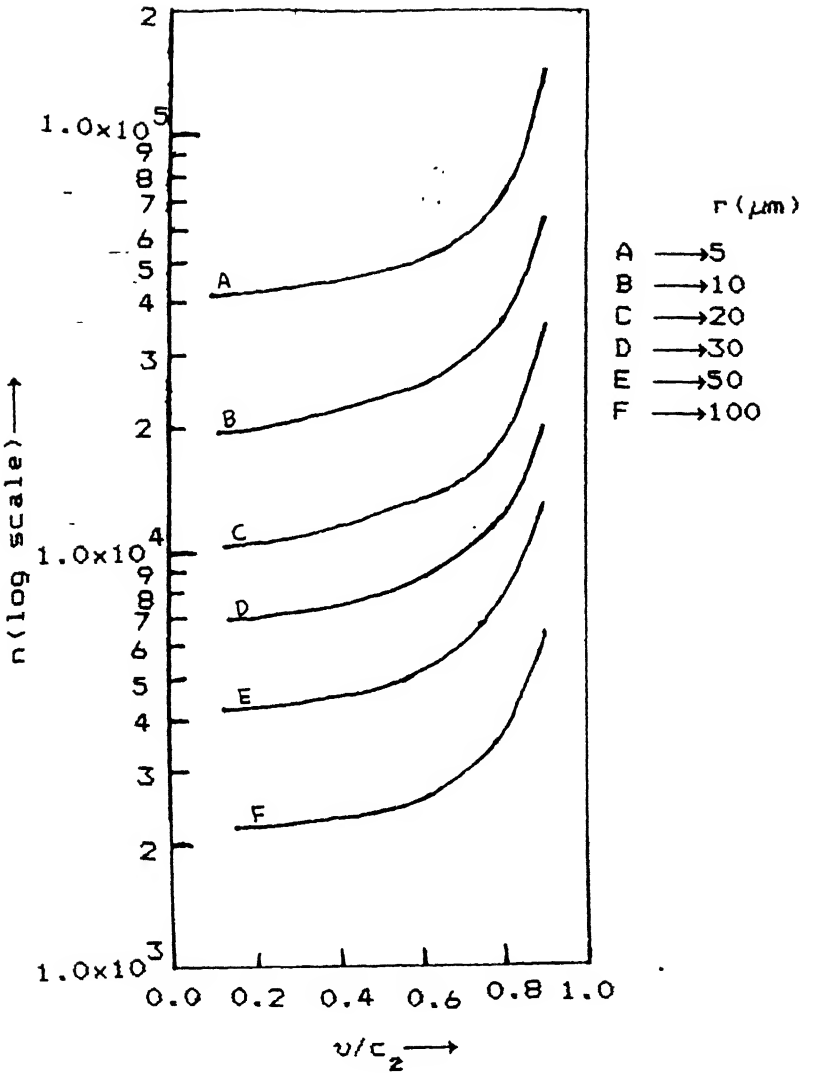

Fig.(2.12) - The variation of number of dislocations(n) with normalized dislocation velocity(υ/c_z) for a fixed crack tip velocity($0.8c_z$) and for radial distance r = 5, 10, 20, 30, 50, 100μm.

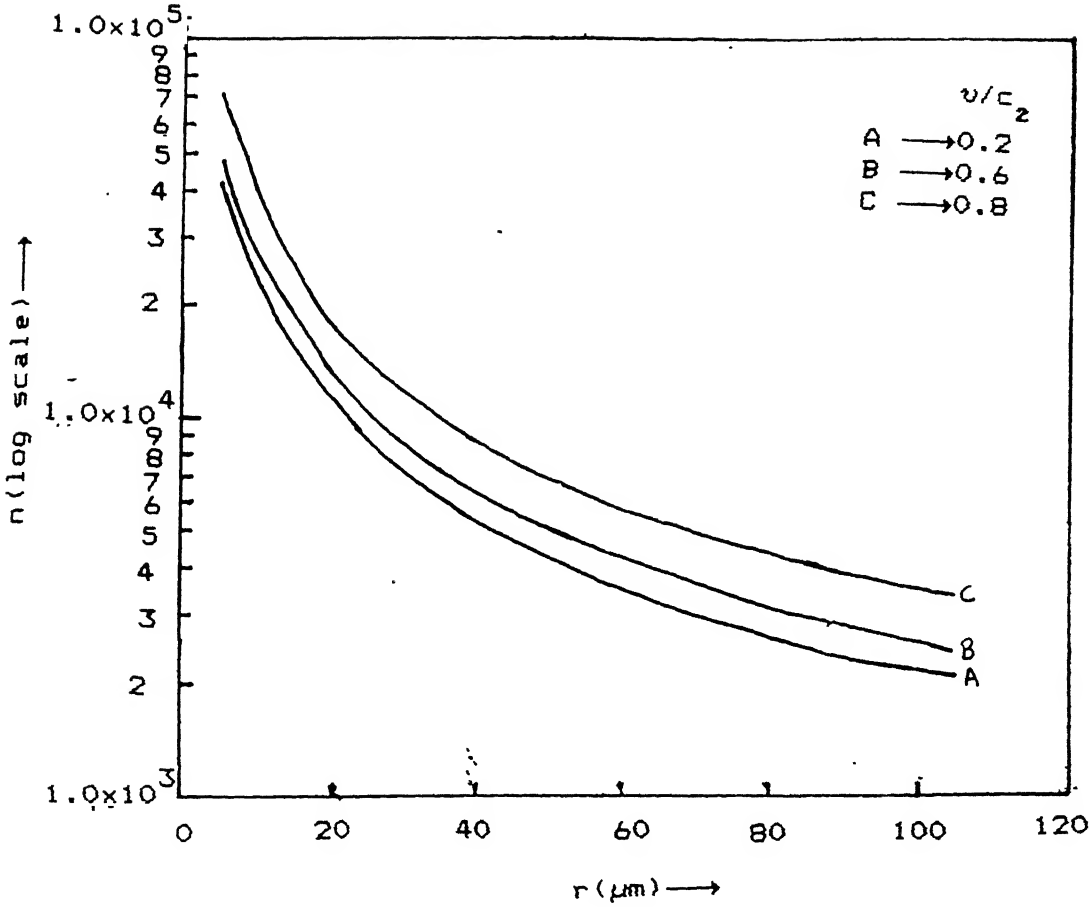

Fig.(2.13) - The variation of number of dislocations(n) with radial distance for a fixed crack tip velocity ($0.8c_2$) and for normalized dislocation velocities 0.2, 0.6, 0.8.

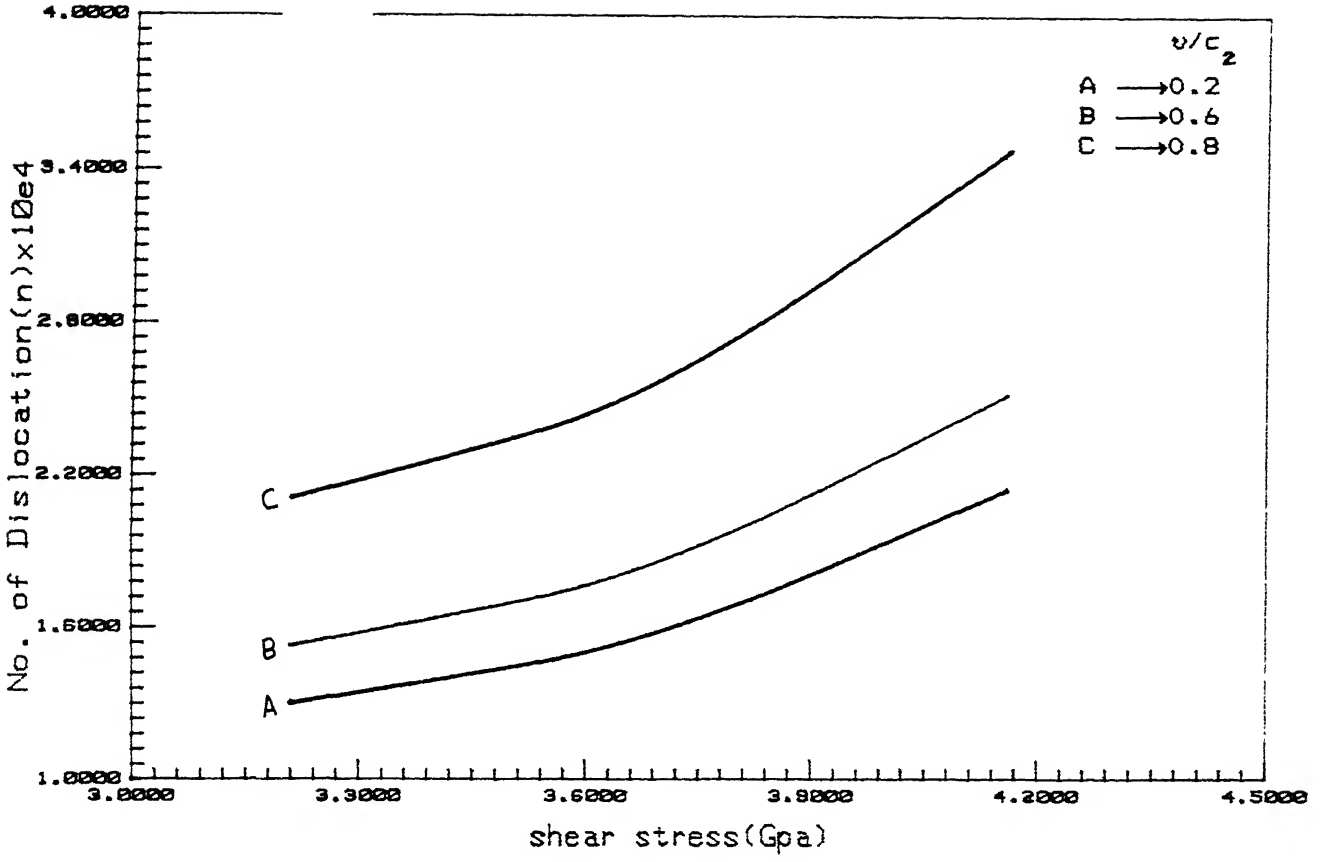

Fig.(2.14) - The distribution of number of dislocation(n) with crack shear stress for a fixed radial distance r = 10μm and for υ/c_2 = 0.2, 0.6, 0.8.

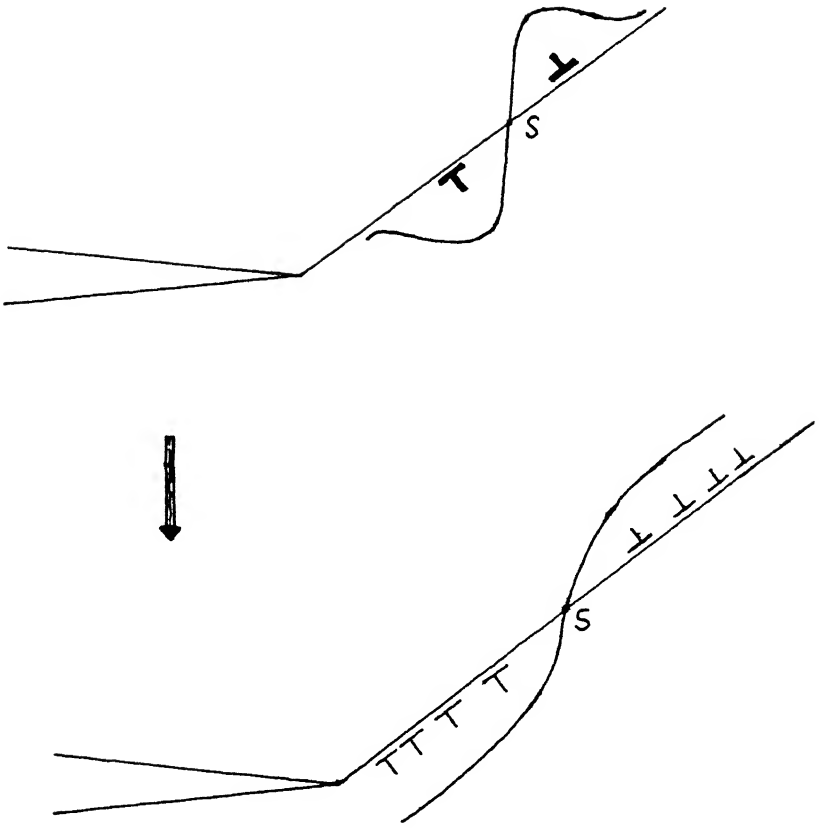

Fig.(2.15) - Showing a giant dislocation of Burger vector nb on the slip plane, splitting into n elementary dislocation. The graph shows a possible distribution function.

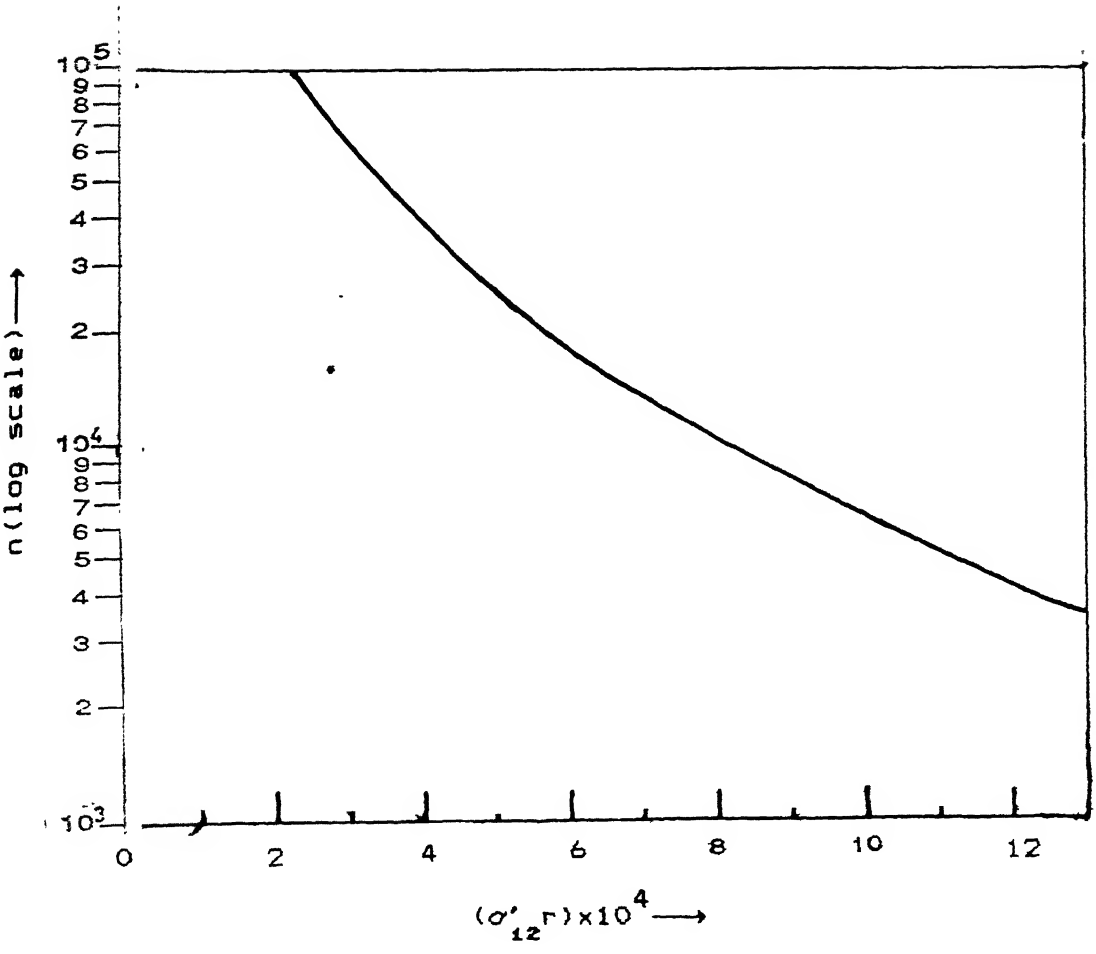

Fig(2.16) - Showing the distribution of dislocations with $(\sigma'_{12}r)$ for $\dot{a} = v = 0.8c_2$.

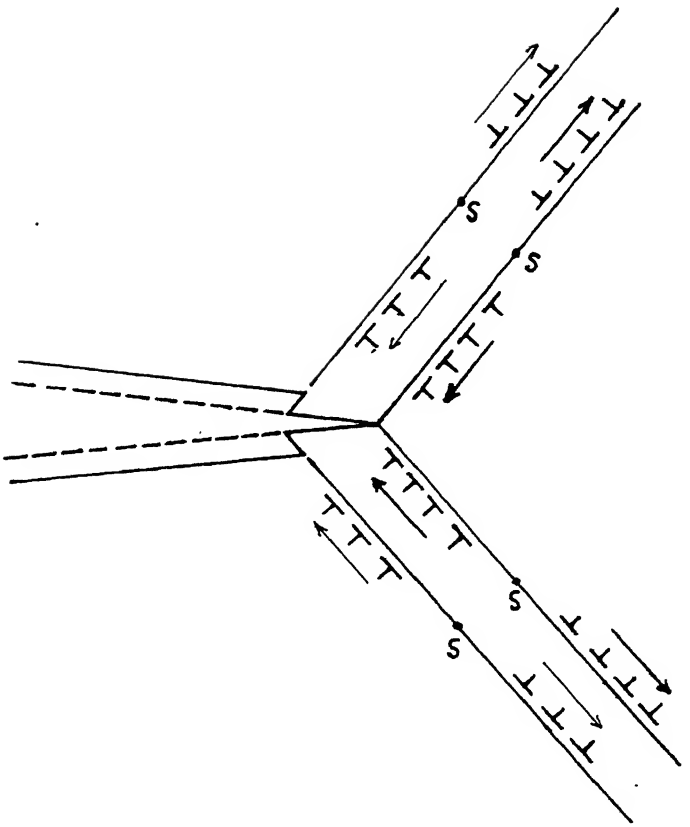

Fig.2.17 Showing the slipped Crack Surface, when dislocations vanish into the crack tip. The active slip planes are shown consistent with Fig. 2.2.

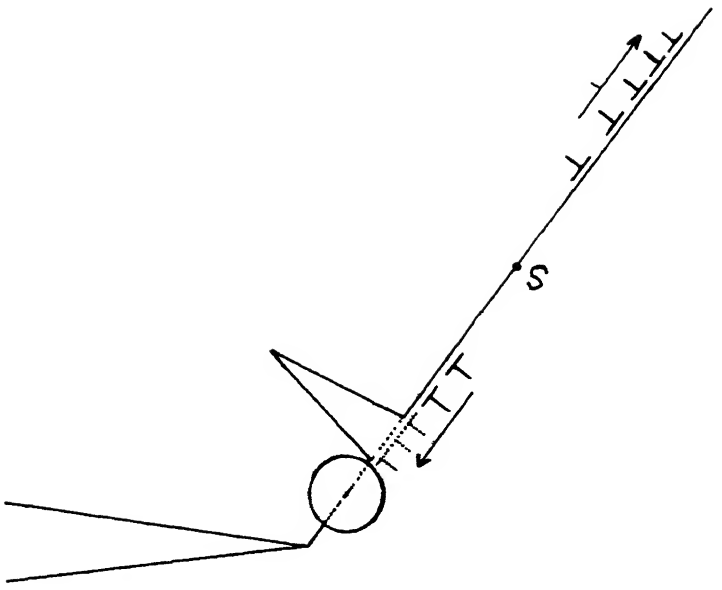

Fig.(2.18) – The formation of a new crack at pile up when both inclusion and matrix are hard. The pile up would vanish into the newly formed crack.

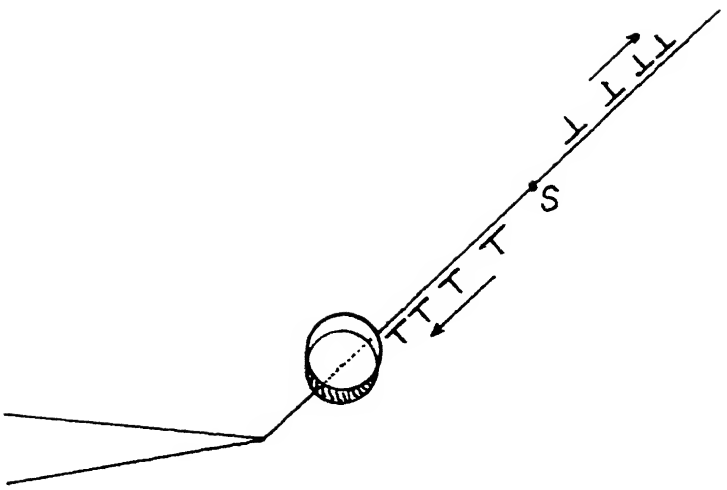

Fig.(2.19) - The formation of void at inclusion and ductile matrix interface, when inclusion is harder than the matrix. The hydrostatic stress field of the piled up is predominently tensile in the upper half of the glide plane and lies in the tensile field of crack.

TABLE NO.2.1 - The nature of maximum force acting on dislocation at different angular positions and normalized crack tip speeds.

$\frac{\dot{a}}{c_2}$	Repulsive force	attractive force
0.0	70	270
0.2	70, 250	110, 290
0.4	-	90, 270
0.6	-	90, 270
0.8	150, 330	30, 90, 210, 270
0.90 - 0.92	140, 320	40, 90, 220, 270
0.94 - 0.99	50, 90, 270	130, 230, 310

TABLE NO.2.2 - The nature of force at different angular position for crack-dislocation-inclusion system.

(+) - Repusive Force

(-) - Attractive force

a/c_2	ϕ = 30	ϕ = 45	ϕ = 60	ϕ = 70
0.0	60^+, 280^+	60^+ 270^+	60^+ 250^+	60^+ 250^+
0.2	70^+ 250^+	60^+ 240^+	60^+ 240^+	60^+ 240^+
	110^- 290^-	120^- 300^-	120^- 300^-	120^- 300^-
0.4	80^+, 260^+	70^+ , 250^+	70^+ , 250^+	60^+ , 240^+
	100^-, 280^-	110^-, 290^-	110^-, 290^-	120^-, 300^-
0.6	90^-, 270^-	90^-, 270^-	90^-, 270^-	80^- , 260^-
				100^+ , 280^+
0.8	150^+ 330^+	150^+ 330^+	150^+ 330^+	340^+
	30^-, 90^-	30^- , 90^-	30^- , 90^-	20^- , 90^-
	210^-, 270^-	210^-, 270^-	210^-, 270^-	160^-, 270^-
				200^-